Dipl.-Ing. Mario Schneeweiß

SEISMIC SAFETY EVALUATION OF THE LUZZONE DAM

MASTER´S THESIS

to achieve the university degree of

Diplom-Ingenieur

Master´s degree programme: Civil Engineering, Geotechnics and Hydraulics

submitted to

Graz University of Technology

Supervisor

Univ.-Prof. Dipl.-Ing. Dr.techn. Gerald Zenz
Institute of Hydraulic Engineering and Water Resources Management

Graz, November 2016

AFFIDAVIT

I declare that I have authored this thesis independently, that I have not used other than the declared sources/resources, and that I have explicitly indicated all material which has been quoted either literally or by content from the sources used. The text document uploaded to TUGRAZonline is identical to the present master's thesis.

Graz, November 2016

....

Mario Schneeweiß

ACKNOWLEDGEMENT

ABSTRACT

The stability of water retention barriers has to be continuously observed and assessed because of the severe consequences of a potential defect. Therefore every barrier has its own measurement program with different methods to notice existing or arising problems in time. Additional to that in situ methods, verification by means of calculations for the assessment of the stability has to be continuously done. Nowadays the most suitable calculation method for the assessment of the stability is the finite element method. Due to the permanent enhancement of the mentioned numerical analysis tool the results are very suitable and helpful to interpret the real dam behaviour.

The investigation of the earthquake behaviour of a double curved arch dam is the subject of this thesis. The analysis of this concrete structure is done with a numerical calculation with the help of the finite element method. The used earthquake loading is simulated with an earthquake time history. This type of consideration of such an earthquake enables the investigation of a nonlinear building response. Another focus of this thesis is the comparison of the results of the used analysis method with results of other scientific calculations respectively analytical methods. The purpose of the comparison is to do a plausibility check which means to ensure that the numerical analyses are as accurate as possible.

Because of operational reasons during construction it is necessary to build concrete dams with independent blocks and therefore step by step. As a consequence of that, block joints arise which have a substantial influence on the total bearing behaviour of the arch dam. Therefore the investigation of the behaviour of the single block during an earthquake is also part of this thesis. In this context the focus is put on the definition of the joint properties because of their crucial influence on the loading behaviour.

The crucial influences on a concrete dam which are considered in this thesis are the properties of the used materials (concrete, rock and water), the contact behaviour between the defined parts (dam, foundation, block and water) and the loadings which are acting on the dam. The static loads applied in the calculations are the self-weight, the water pressure, the loading due to sedimentation and the thermal influence of the annual seasons. As mentioned above the dynamic loads in a seismic event are considered with an acceleration time history. To get realistic results regarding the dam behaviour in case of a dynamic excitation also the interactions between the parts are defined.

All in all it can be said that the comparison of numerical calculations of the double curved arch dam for two different mesh sizes (calculation for the publication and for this thesis) results in a similar observation. Small deviations occur at the comparison of the displacements. The reason for the deviation lies in the consideration (in the calculations of the publication) respectively the non-consideration (calculations for this thesis) of the acoustic impedance at the reservoir´s side faces and the bottom face. Also the results for the natural frequencies and the natural modes are compared and coincide.

The evaluations from the calculation with the numerical model which includes the defined single block show that the system does not fail. This is proved by analysing the contact pressure in the block joints which is sufficient throughout the whole earthquake event.

Finally an evaluation of the acceleration at the crest shows that the ground excitation at the base of the dam is amplified 18 times at the crest. This amplification occurs for the upstream and downstream direction.

KURZFASSUNG

Auf Grund ihrer Schadensfolgewirkung werden Talsperren stets bezüglich ihrer Standfestigkeit beurteilt. Dazu gibt es für jedes Dammbauwerk eigene Mess- und Überwachungsprogramme, bestehend aus unterschiedlichen Messmethoden, um frühzeitig vorhandene oder entstehende Probleme erfassen und darauf reagieren zu können. Zusätzlich zu diesen in situ Methoden werden parallel dazu Beurteilungen durch Berechnung der statischen Standsicherheit durchgeführt. Die in der heutigen Zeit am weitesten verbreitete Berechnungsmethode ist jene mit Hilfe der Finiten-Elemente-Methode. Durch numerischen Analysetools sind die Ergebnisse sehr hilfreich und gut geeignet, um das „reale Verhalten" interpretieren zu können.

Ziel dieser Arbeit ist die Untersuchung einer doppelt gekrümmten Bogenstaumauer in Bezug auf ihr Erdbebenverhalten. Die Analyse dieses Betonbauwerkes erfolgte mit Hilfe einer numerischen Berechnung in Form der Finiten-Elemente-Methode. Die dieser Analyse zu Grunde liegende Erbebenbelastung wurde durch Erdbebenzeitverläufe simuliert. Diese Art der Erbebenberücksichtigung ermöglicht es, ein nichtlineares Verhalten des untersuchten Staubauwerkes zu erfassen. In dieser Arbeit wurde zusätzlich großes Augenmerk auf den Vergleich der Ergebnisse mit Berechnungen aus anderen wissenschaftlichen Arbeiten sowie aus eigens angestellten analytischen Berechnungen gelegt, um die größtmögliche Sicherheit bezüglich der Aussagekraft der Analysen zu erhalten. Ein solches Vorgehen wird auch Plausibilitätscheck genannt.

Aus baubetrieblichen Gründen können Staudämme aus Beton nur in Blöcken, beziehungsweise abschnittsweise gefertigt werden. Die dadurch entstehenden Blockfugen haben einen erheblichen Einfluss auf das Gesamttragverhalten eines derartigen Bauwerkes. Die Untersuchung des Verhaltens eines einzelnen Blockes während eines Erdbebens ist ebenfalls Teil dieser Arbeit. Besonderes Augenmerk wurde hierbei auf die Definition der Blockfugeneigenschaften gelegt, da diese hauptausschlaggebend für die Berechnungsergebnisse sind.

Die ausschlaggebenden Einflüsse auf eine Staumauer aus Beton, welche in dieser Arbeit berücksichtigt sind, sind die Eigenschaften der verwendeten beziehungsweise vorhandenen Materialien (Beton, Fels und Wasser), das Verhalten der sich berührenden Teile (z.B. Staumauer und Wasser), sowie die auf das Dammbauwerk wirkenden Belastungen. Die in den Berechnungen berücksichtigten statischen Einwirkungen sind das Eigengewicht, der Wasserdruck, die Belastung auf Grund von Sedimentation und der sich aus den Jahreszeiten ergebende thermische Einfluss. Wie oben erwähnt, ist die dynamische Belastung durch ein Erdbeben mittels Beschleunigungszeitverläufen berücksichtigt. Um ein realitätsnahes Ergebnisse bezüglich des Staudammveraltens bei Erdbebenbelastung zu erhalten, sind auch die Interaktionen zwischen den einzelnen Bauteilen definiert.

Zusammenfassend ist zu sagen, dass die numerische Berechnung der doppelt gekrümmten Bogenstaumauer mit zwei unterschiedlichen Netzgrößen (wissenschaftliche Veröffentlichung sowie die Berechnungen für diese Arbeit) die im Wesentlichen gleichen Resultate ergibt. Geringfügige Abweichungen ergeben sich beim Vergleich der Verschiebungen. Der Grund für diesen Unterschied ergibt sich aus der Berücksichtigung (in den Berechnungen der

Veröffentlichung) beziehungsweise der Nichtberücksichtigung (Berechnungen für diese Arbeit) des akustischen Scheinwiederstandes an den Reservoirseitenflächen und an der Reservoirsohle. Zusätzlich ist der Vergleich der Eigenfrequenzen und der Eigenformen angestellt worden. Hierbei sind keine Abweichungen zu beobachten.

Die Auswertungen der Berechnungen mit der Berücksichtigung des definierten Einzelblockes zeigen kein Versagen des Systems. Dies ist durch die Analyse des vorhandenen Kontaktdruckes in den Blockfugen dargelegt. Hierbei ist während der Erbebenbelastung stets genügend Druckspannung vorhanden.

Abschließend zeigt die Auswertung der Beschleunigung an der Dammkrone einen Verstärkungsfaktor von 18 gegenüber der Erdbebenanregung am Fußpunkt. Dieser Verstärkungsfaktor hat sowohl stromaufwärts als auch stromabwärts Gültigkeit.

CONTENT

1 Introduction and motivation

The collapsing of a water retention structure would be the worst case scenario. The damage can affect a large area with material harm and also hurt or rather kill many people. Because of its high risk potential the calculation of the behaviour during static and dynamic loading is essential for the assessment of the stability for safety. The development of new calculation methods and new calculation approaches respectively the improving of them enhance the calculation results. Therefore the assessment of safety is a continuous process over many years. The dynamic loading respectively the earthquake loading is the main influence in connection with this hazard evaluation.

For a stability analysis of concrete dams the finite element method is a common tool to be used. By using this numerical method results with high confidence can be achieved. Numerical calculations can be either linear computations or non-linear calculations. The earthquake loading under linear system response is based on quasi static earthquake loads, modal superposition or time history. For consideration of non-linear effects of material properties, contact problems or geometric non linearity a time acceleration history analysis is required. In both numerical calculation methods the variation of different parameters can result in evaluations which deviate significantly from each other. Therefore every numerical calculation has to be checked for its plausibility.

The calculations (of this thesis) of the static and dynamic behaviour for the pictured double curved arch dam is based on the provided data for a benchmark workshop in Switzerland. The instructions of this benchmark workshop were headlined "Seismic Safety Evaluation of Concrete Dam Based on Guidelines". The present thesis shows the behaviour against loading of the depicted arch dam below. Additionally also the behaviour of a single block is investigated.
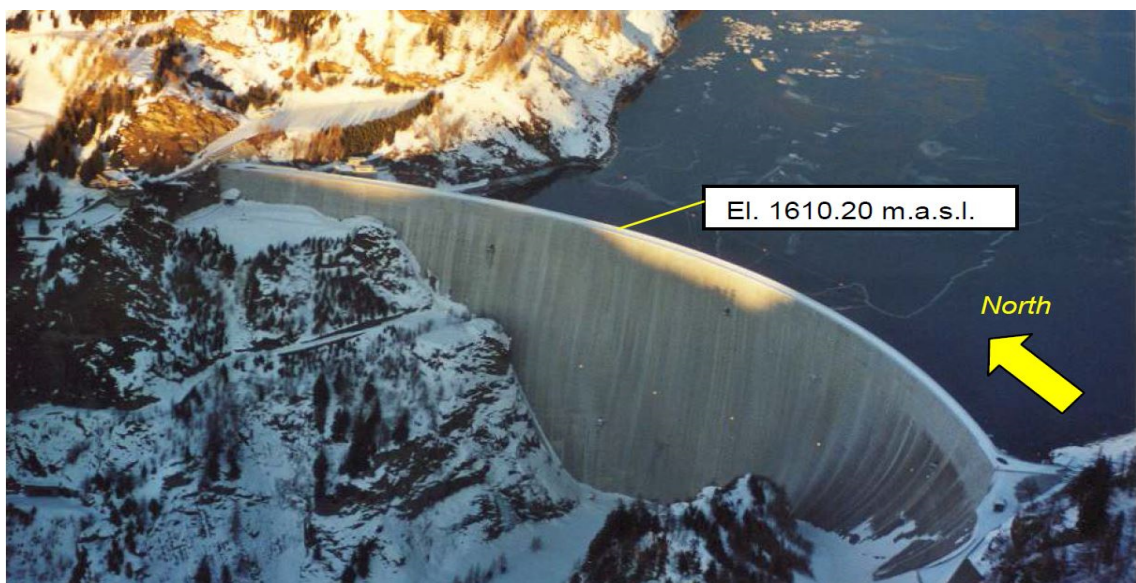
Figure 1-1   Luzzone Dam (Switzerland), H=225 [m] (source: [4])

2 System conditions for the dam under investigation

The "Luzzone" dam is a retention structure with a total height of 225 [m] in the canton Tessin (in Figure 2-1 shown in different shades of orange) in the Italian speaking part of Switzerland. Its location is shown in Figure 2-1 highlighted with the red arrow. This region is located in the southern part of the country. The present double curved dam is characterised by a crest length of 530 [m] and a crest width of 4,55 [m]. The concrete thickness at the foundation is about 36 [m]. The storage capacity of the "Lago di Luzzone" (Figure 2-2) which results of the damming is 107 [Mm³] at normal water level.

Figure 2-1   Map of the canton Tessin which shows the location of the dam (source: [8])

The dam was completed in 1963 after a building time of about 5 years. At that time the total height of the arch dam was 208 [m]. In 1997-1998 the capacity of the system was increased by 25 % by heightening the dam. After one year building time the construction was 17 [m] higher and has now a total height of 225 [m]. The concrete used for this enlargement has different properties in comparison to the old one which was used in the 1960s (chapter 5.3.2). It should be noted that the newer one has lower properties than the older one. This difference is considered in the finite element model to be able to assess the structural behaviour.

Figure 2-2 shows the "Lago di Luzzone" with a lowered water level. The line between the brown parts of the slope without grass and the green area of the slope shows the maximum water level and is called shore line (black line in Figure 2-2). The total height of the crest of the arch dam is at 1610 [m.a.s.l.] and with consideration of the freeboard the normal water level is at 1606 [m.a.s.l.]. Because of that the borderline between the brown area and the green area in Figure 2-2 is situated 1606 [m] above sea level. In the picture below the water level is approximately at 1550 [m.a.s.l.].

Figure 2-2   Lago di Luzzone (source: [7])

Side note: On the airside of the concrete dam more than 160 climbing handles are mounted which makes this trail the longest man-made climbing trail in the world.

3 Principle of dynamic analysis

Herein the principles used in the following chapters are laid down.

3.1 Principle of the Multi-Mass Oscillator

The following explanations are based on source [1].

Multi-Mass Oscillators are often used in calculations of buildings to identify their susceptibility to dynamic action. These calculations describe the interaction of masses which are arranged in series and connected with linear springs (multi degree of freedom → MDOF). For example, the total masses of each floor of a tower will be concentrated in one point, usually at the level of its ceiling. These individual mass points have different heights h with different masses m and different displacements u.

Subsequently the way from the equations of motion for each floor to a system of equations displayed in matrices is shown.

$$m_1 * \ddot{u}_1 + \sum_{j=1}^{n} c_{1j} * \dot{u}_j + \sum_{j=1}^{n} k_{1j} * u_j = p_1(t) \tag{3-1}$$

$$m_2 * \ddot{u}_2 + \sum_{j=1}^{n} c_{2j} * \dot{u}_j + \sum_{j=1}^{n} k_{2j} * u_j = p_2(t) \tag{3-2}$$

$$\vdots$$

$$m_n * \ddot{u}_n + \sum_{j=1}^{n} c_{nj} * \dot{u}_j + \sum_{j=1}^{n} k_{nj} * u_j = p_n(t) \tag{3-3}$$

$$[M]\{\ddot{U}\} + [C]\{\dot{U}\} + [K]\{U\} = \{P(t)\} \tag{3-4}$$

Equation of Motion written in matrices.

Explanation of the different matrices which are used for the equation of motion:

The mass-matrix below contains the masses of all "mass-points" of the existing system and is defined as a diagonal matrix. In case of a tower the concentrated masses of the individual floors are written on the diagonal. This type of matrix is a so called lumped mass matrix (3-5). In contrast the mass could also be written as a consistent mass matrix (3-6). In that type of matrix also other places in the matrix than the diagonal ones are taken and all masses are influenced by each other. The calculation of a consistent mass matrix needs more numerical effort.

Lumped mass matrix

$$[M] = \begin{bmatrix} m_1 & 0 & \cdots & 0 \\ 0 & m_2 & & 0 \\ \vdots & & \ddots & \vdots \\ 0 & 0 & \cdots & m_n \end{bmatrix} \tag{3-5}$$

Consistent mass matrix

$$[M] = \begin{bmatrix} m_{11} & m_{12} & \cdots & m_{1n} \\ m_{21} & m_{22} & & m_{2n} \\ \vdots & & \ddots & \vdots \\ m_{n1} & m_{n2} & \cdots & m_{nn} \end{bmatrix} \tag{3-6}$$

The stiffness matrix contains the stiffness behaviour of the existing system.

For example: k_{21} means the effect on the stiffness behavior of point two in the event of load case one.

Stiffness matrix

$$[K] = \begin{bmatrix} k_{11} & k_{12} & \cdots & k_{1n} \\ k_{21} & k_{22} & & k_{2n} \\ \vdots & & \ddots & \vdots \\ k_{n1} & k_{n2} & \cdots & k_{nn} \end{bmatrix} \tag{3-7}$$

The damping matrix contains the damping behaviour of the existing system.

For example: c_{21} means the effect on the damping behavior from point two in the event of load case one.

Damping matrix

$$[C] = \begin{bmatrix} c_{11} & c_{12} & \cdots & c_{1n} \\ c_{21} & c_{22} & & c_{2n} \\ \vdots & & \ddots & \vdots \\ c_{n1} & c_{n2} & \cdots & c_{nn} \end{bmatrix} \tag{3-8}$$

Explanation of the three different vectors which are used for the equation of motion:

The vectors are the displacement $\{U\}$, the velocity $\{\dot{U}\}$ and the acceleration $\{\ddot{U}\}$ of the defined points.

$$\{U\} = \begin{bmatrix} u_1 \\ u_2 \\ \vdots \\ u_n \end{bmatrix}; \{\dot{U}\} = \begin{bmatrix} \dot{u}_1 \\ \dot{u}_2 \\ \vdots \\ \dot{u}_n \end{bmatrix}; \{\ddot{U}\} = \begin{bmatrix} \ddot{u}_1 \\ \ddot{u}_2 \\ \vdots \\ \ddot{u}_n \end{bmatrix} \tag{3-9}$$

$$\dot{u}_n = \frac{\partial_{u,1}}{\partial_t}; \ \ddot{u}_n = \frac{\partial_{u,2}^2}{\partial_t^2} \tag{3-10}$$

3.2 Differentiation of dynamic actions (source: [1])

There are different options to describe the effect of dynamic actions on buildings. The following variants show the possible time flows of a dynamic load. On the abscissa of each diagram the time is applied and on the ordinate the displacement.

3.2.1 Harmonic Action
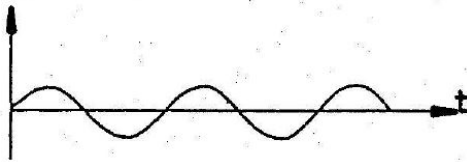
Figure 3-1   Harmonic Action (source: [1])

After energizing a component and waiting for a long enough time the energized part acts harmonic. This is because of everything's internal damping. After waiting infinite long time the rest of the energized waves are only stationary waves.

Harmonic energized waves are acting after infinite long time sinusoidal.

3.2.2 Periodic Action
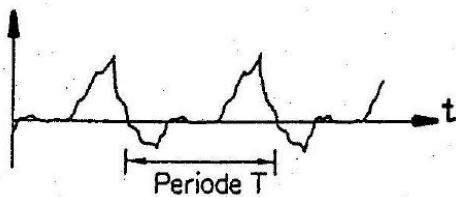
Figure 3-2   Periodic Action (source: [1])

"Periodic" means returning after a period of time T. Periodic waves could be described with a Fourier analysis. The acting time lasts for so long that the building starts to swing stationary.

Excitations could be:

- Running or walking
- Wind
- Rotating masses with oscillating parts or imbalanced rotating parts

3.2.3 Transient Action
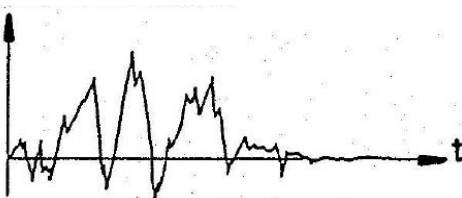
Figure 3-3   Transient Action (source: [1])

Transient waves show no periodicity and have any time flow. Every acting time of the energizing load is possible. It is possible to approximate transient waves with a Fourier analysis.

Excitations could be:

- Wind
- Earthquake

3.2.4 Pulsed Action
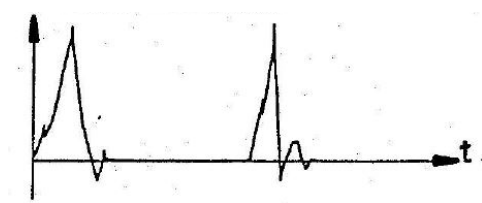
Figure 3-4   Pulsed Action (source: [1])

A pulsed action is basically the same as a transient action but the building response is a little bit different. This is because of its time of exposure.

Excitations could be:

- Explosions
- Impact of cars or other vehicles
- Construction work (e.g. ramming of a sheet pile wall)

3.3 Modal dynamic analysis

3.3.1 Modal analysis

The modal analysis describes the dynamic behaviour of structures. The results of this analysis are natural frequencies and natural modes. Every natural mode has a corresponding natural frequency. This values are essential in the design phase of a structure to optimise its dynamic behaviour. By means of a modal analysis an assessment of the dynamic behaviour can only be qualitative. A quantitative interpretation is not possible. The building response of a structure is always the superposition of some natural modes.

3.3.2 Response spectrum

Basically there are three different types of response spectrums, namely displacement, velocity and acceleration response spectrums. The response spectrum displays the maximal building response with dependence to the natural frequency and the damping. For example regarding an arch dam the maximum acceleration due to an earthquake excitation can be directly read out of a response spectrum (for a selected natural frequency).

The following picture shows exemplarily the response spectrum of the earthquake in EL Centro in 1940. Because of the relationship (approximately) between all factors the response spectrum can be written as a so called tripartite diagram (Figure 3-5). On the abscissa the natural frequency/vibration and on the ordinate the responded velocity of the building is written. The crossed lines are the acceleration and the deformation of the building. The thick black lines are the building response calculated with 0, 2, 5, 10 and 20% damping.

Figure 3-5   Exemplary response spectrum for EL Centro ground motion with $\xi = 0, 2, 5, 10,$ and 20% (source: [15])

3.3.3 Theoretical background of the used Rayleigh damping factors

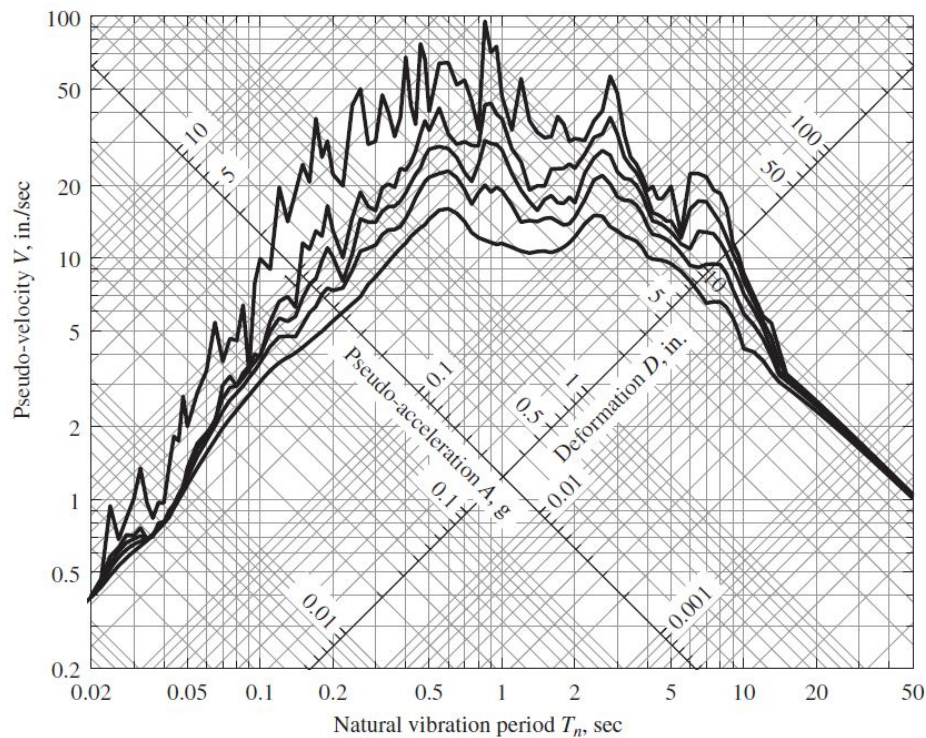*"Damping in mechanical systems, especially in the equation of motion, is defined as a velocity dependent quantity (viscous damping), which describes the dissipation of energy during a dynamic oscillation. Damping factors are hard to define for even simple structures. In case of civil engineering structures, where each structure is more or less a prototype, the damping is not known in the design phase. Due to the complexity of some structures and their interaction with the soil or water and the use of different materials it's almost impossible to account for all damping effects separately. Consequently one may use values measured at similar structures, which can be found in relevant literature."* [2]

For the damped equation of motion (formula (3-4)) a damping matrix is necessary. To define this matrix the Rayleigh damping is used. The Rayleigh damping is based on the modal analysis developed by Lord Rayleigh in 1877. It says that the mass and stiffness matrices of an undamped structure have an orthogonal relationship. Therefore a system with multiple degrees of freedom can be fragmented into a compilation of systems with one degree of freedom. The Rayleigh damping, also called the proportional damping, uses the undamped mass and stiffness to converge the viscous damping with a linear combination.

As mentioned above the following formula (Rayleigh damping) is a combination of the mass (indicated with M) with its according α-value and the stiffness (indicated with K) with its according β-value. α and β are constants and can be calculated as mentioned below.

$$C = \alpha * M + \beta * K \qquad (3\text{-}11)$$

The subsequent formulas show the calculation of the constants α and β which are necessary for the calculation of the Rayleigh damping. α stands for the so called mass-proportional factor and β for the so called stiffness-proportional factor. The also used modal damping ξ_i is a material, structural and soil depending factor. For the calculation of both factors (α and β) two natural frequencies are necessary which have to be chosen by the calculators. The fact that the frequencies have to be chosen can be regarded as a disadvantage.

$$\alpha = \xi_i * \frac{2 * \omega_i * \omega_j}{\omega_i + \omega_j} \qquad (3\text{-}12)$$

$$\beta = \xi_i * \frac{2}{\omega_i + \omega_j} \qquad (3\text{-}13)$$

Figure 3-6 shows the depiction of the Rayleigh damping. On the abscissa of the subsequent diagram the natural frequency is written and on the ordinate the critical damping of the used structure, material or soil. The dotted and the dashed line represent the mass-proportional and the stiffness-proportional damping. The continuous line is the Rayleigh damping which is the linear combination of the mass- and stiffness-proportional damping (formula (3-11)). As you can see in

the diagram the choice of the frequencies respectively the chosen range is essential for the result of the calculation of the constants and furthermore for the FE-calculation. The subsequent diagram also shows that the Rayleigh damping above and below the chosen natural frequencies range (between ω_i and ω_j) is higher than between them. Furthermore that means that a small range results in a big damping and a big range in a small damping. This fact is definitely the biggest disadvantage of this method.
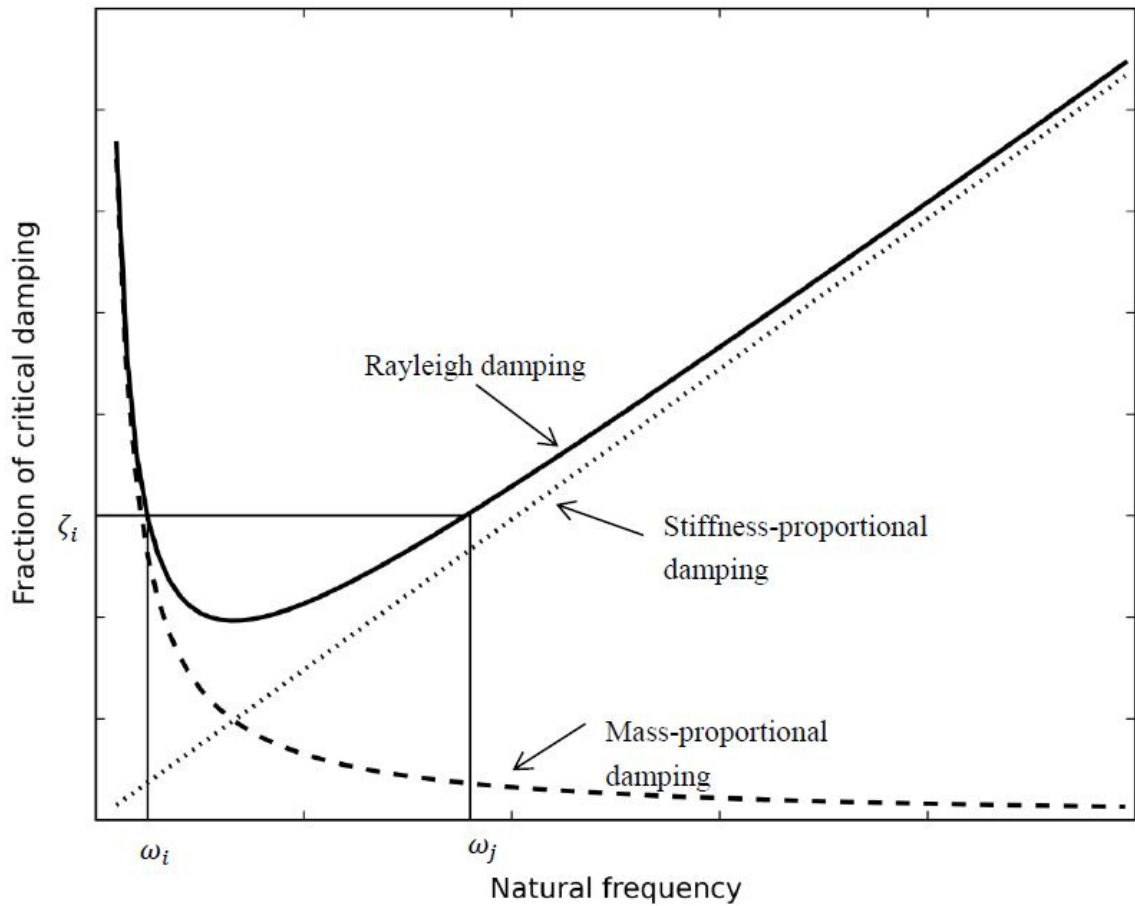

Figure 3-6   Depiction of Rayleigh damping (source: [2])

4 Overview of concrete dams and their foundations

4.1 Different kind of dams

Concrete dams are usually categorized into four types. The following part gives a short description of these dams which are shown in Table 4-1. The type of the retention structure used for this thesis is a double curved arch dam.

- Gravity dam: In Table 4-1 in the third column (named "geological") it is shown that this type of dam has to be built on rocks, which have to have enough bearing capacity to carry high concentrated loads from the whole construction. The gravity dam countervails the pressure of the water only with its own weight and the friction resistance in the slip joint.
- Buttress dam: The characteristic of this dam type is that the dam wall is supported by triangular buttresses.
- Arch dam: Arch dams can be subdivided into two groups. One subgroup consists of the conventional arch dams and the other of the double curved arch dams. Regarding the conventional arch dams the curvature can only be seen in the layout drawing. The name of the second one tells that there are two curvatures which can be seen in the layout drawing and also in the vertical projection of the dam. To derive the forces which are acting on the dam, the flanks of the valley should have a very competent rock. In comparison to the gravity dam the arch dams have many advantages regarding their volume and they have a better utilization of the concrete quality respectively the concrete strength.
- Arched gravity dam: This type of dams combine the advantages of the gravity and arched dams. It is important to know that this dam type needs a high bearing capacity at the floor and also at the flanks of the valley.

The following table gives an overview of the mentioned types of concrete water retention barriers with their relative field of application and their geological requirements and their particular functionality.
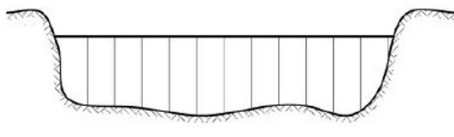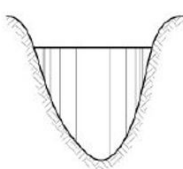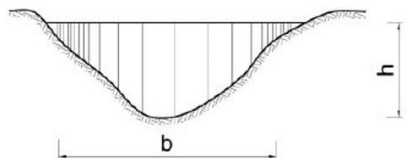
Dam type	Topological		Geological	Load carrying action
	Requirement			
Gravity dam	Field of application: Wide valley		Sustainable rock of the valley bottom	Self-weight
Buttress dam			Sustainable rock of the valley bottom with a constant modulus of elasticity	
Arch dam	Field of application: Narrow U- or V-valley with steep flanks		Constant sustainable rock with a high deformation modulus especially at the flanks	Arched shape
Arched gravity dam	At valleys with b/h < 5		Sustainable rock of the valley bottom and flanks	Self-weight and arched shape

Table 4-1   Different types of concrete dams (source: [3])

4.2 General requirements for the dam foundation

Gravity dams and arch dams have to be founded on competent rock because of the required bearing capacity of the foundation and the permeability. The structure of the rock mass is predetermined by nature and can only be adapted for the desired application. This fact distinguishes rock mechanical calculation from construction engineering. In construction engineering the properties of the different working materials are known because mostly they are fabricated or adapted for their predetermined use. As mentioned above in rock engineering the properties of the working material (rock) are given by nature and so only improvements for example by means of excavation or grouting are possible.

Important properties of the foundation of dams are:

- Permeability
- Bearing capacity
- Deformability
- Structure (e.g. layering of material) and
- Composition

The properties of the rock mass at the footprint and the banks of the arch dam are essential to guarantee the stability of the dam.

The geotechnical engineer has to determine joints, faults, the strength and the deformability of the present rock. This has to happen in a depth which corresponds approximately with the height H of the dam and in a radius of 1xH around the dam. This area around the projected dam is depicted in the following figure.
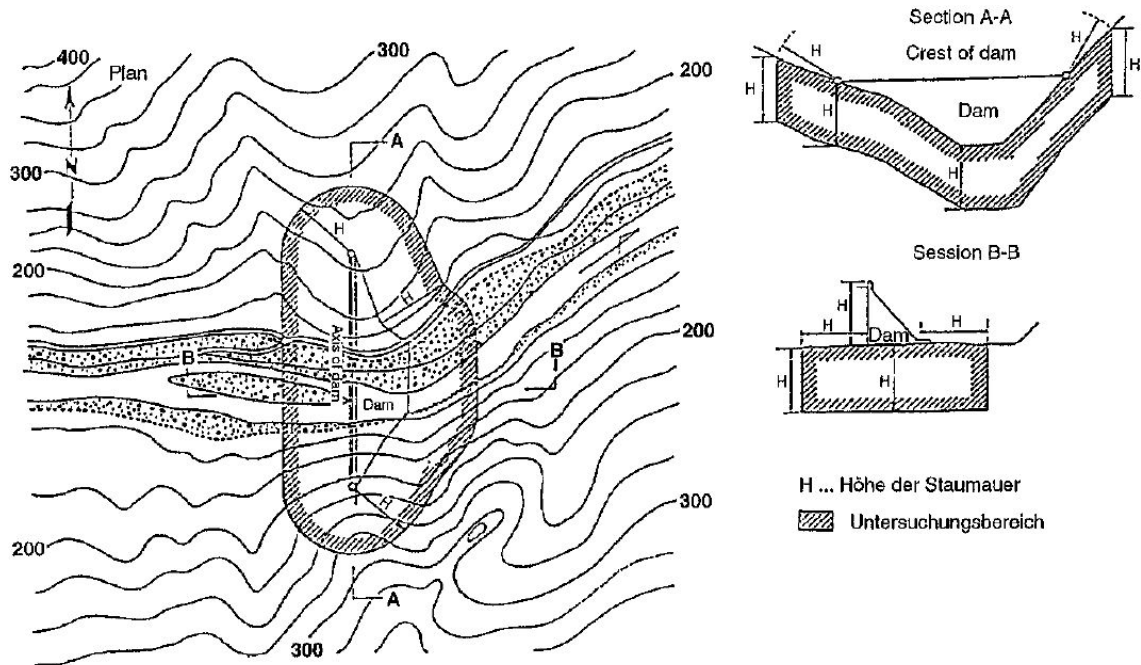
Figure 4-1   Area of investigation for the assessment of the eligibility of the ground for the founding of a dam (source: [12])

Investigation methods for the examination of the above pictured area can be for example geological maps for a general overview of the existing conditions as well as aerial photographs, core drills or seismic methods. The choice of the investigation method and the area of investigation are to be based on joint decisions of geotechnical and dam engineer and should give a good picture of the present conditions. Beforehand a concept regarding the distribution of the bearing-load into the foundation is needed respectively has to be developed.

4.3   Arch dam construction

The dam material is concrete. The quality of the concrete and the economic feasibility of the project depend on construction operating aspects. Main factors for the economic feasibility are the distances between the mining area of the aggregates, the production area of the additives and the building area. The operating factors are mainly influenced by the production and the transport of the fresh concrete.

For practical construction operation reasons the dam has to be concreted in blocks. Also chemical influences, mainly the environmental temperature in combination with the hydration temperature, determine the construction method. The so called "hydration temperature" arises during the hardening process of the concrete. To reduce this temperature and therefor reduce the likelihood of cracking of concrete during the hardening process the block height needs to be reduced or crashed ice has to be added to the water used for the concrete. Also a cooling system could be integrated in the block which accelerates the dissipation of the hydration temperature and furthermore reduces the temperature difference between the border face and the core of the concreted block. In addition the cooling system reduces the temperature of the concrete block faster and therefore shortens the time until block joint grouting is possible.

Because of the construction process block joints form. To ensure that arch dams act as a monolith, grouting mortar has to be injected into the joints. Due to the importance of the injection relating to the total dam behaviour, for every arch dam particularly coordinated injection programs have to be applied. Also particular monitoring programs for the verification of the correct injection process have to be established.

To get results of the numerical calculations which are in accordance with reality it is necessary to define all forces which are acting on the dam. It has to be distinguished between static and dynamic actions. Depending on whether action needs to be considered the material characteristics are different. The following chapters describe all data (static and dynamic) used for the calculations of this thesis.

5 Data used for the calculations

5.1 Geometry and finite element model of the calculated arch dam

The following points describe the way from the basic numerical model to the model which is used for the numerical calculations in this thesis.

5.1.1 Provided basis for the numerical model

The basis of all calculations in this master´s thesis is an orphan mesh (original mesh) which was generated with the program DIANA (DIsplacement ANAlyzer) and provided by the formulators of the benchmark workshop [4]. This finite element software is comparable to the program Abaqus which is used for all the calculations in this thesis. The orphan mesh is provided by the authors of the benchmark workshop. Abaqus Documentation describes the orphan mesh as follows: *"A collection of nodes, elements, surfaces, and sets with no associated geometry. In effect, the mesh information has been orphaned from its parent geometry. You can import a part into Abaqus/CAE from an output database or from an input file in the form of an orphan mesh."* [5]

The following picture shows the basic model which is provided by the authors. This model has only topographical information. Therefore no material data, interaction information or anything else is implemented in the provided model. All these definitions (for example material characteristics or any dynamic characteristics) have to be defined and are explained in the following chapters.
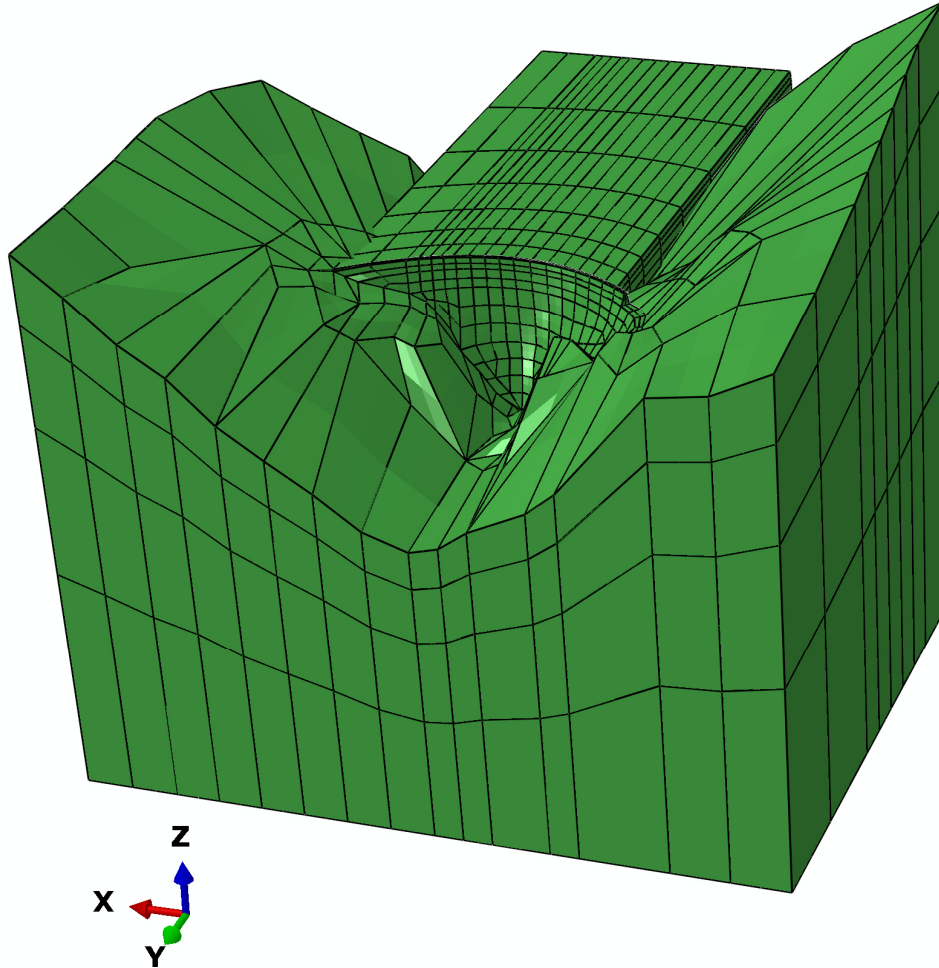

Figure 5-1   Basic model which is the basis for all calculations

5.1.2 Description of the numerical model used for the calculations where the subdivision of the dam into blocks is neglected

In a first step the rough mesh has to be refined to increase the precision of the calculation. This should help to improve the calculation results. Due to the refined mesh the calculation time increases. The following picture shows a comparison between the basic model (left part of the picture) and the refined model (right part of the picture). As you can see in the red circled area only the mesh of the dam is refined. This is because only the calculation results of the double curved arch dam are of interest for this thesis and the influence of the mesh size regarding the other parts (foundation and reservoir) is insignificant.

It also has to be said that the method of construction is neglected in the basic model. The steps of construction of an arch dam are explained in more detail in chapter 4.3 "Arch dam construction". The investigation of the stability of an exemplary model block is also a main part of this master´s thesis. To investigate the behavior of this model block the basis model has to be adapted. Because of this adaption block joints form. This adaption of the basic model is explained in more detail in the next chapter 5.1.3.
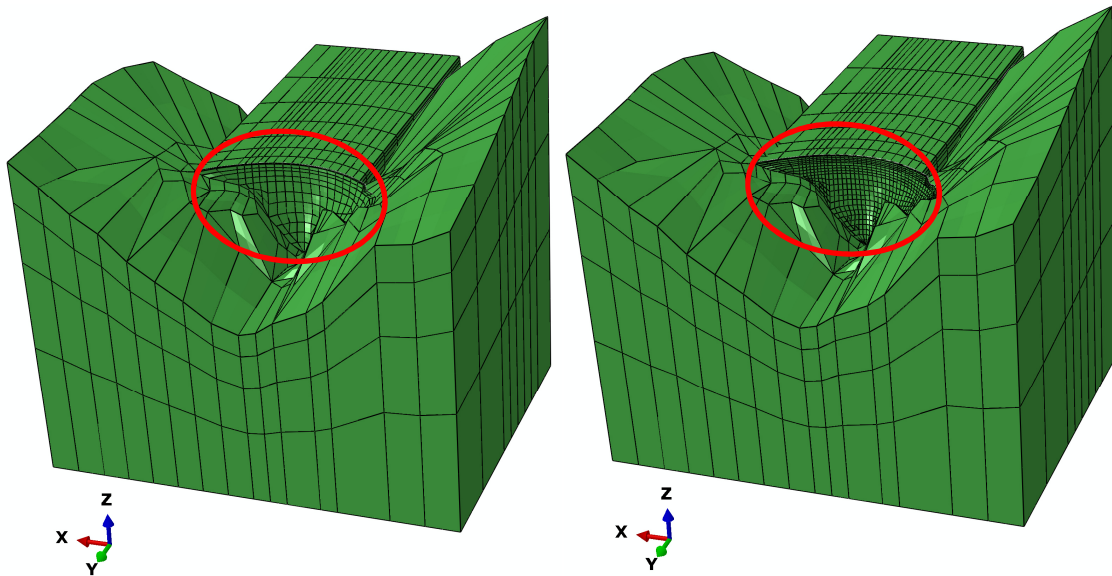

Figure 5-2   Comparison between the basic model (left part of the picture) and the model with the refined arch dam (right part of the picture)

Defining the material characteristic was the second step but this is explained in more detail in chapter 5.3. To guarantee the functionality of the model the boundary conditions and the interactions between the parts had to be defined additionally (see chapter 5.2).

All calculations of this thesis are calculated with a time history and are solved implicitly.

5.1.3 Description of the numerical model where the block design is considered in form of one exemplary model block

As said in chapter 4.3 arch dams consist of blocks to enable their construction and because of the material properties respectively the material behavior of the concrete. Due to the building technique construction joints (block joints) occur. In case of an earthquake these block-joints may open due to tensile stresses and one or more blocks could overturn or slide out. To analyze this behavior a single model block as shown in Figure 5-3 on the left picture side is chosen. The interaction between this block and the dam is defined in chapter 5.2.2.

In Figure 5-3 a general overview of the finite element model including a detailed view of the considered block is depicted. The height of the defined block is 100 [m] its width is 20-23 [m] (see the picture on the right side below). Its exact location is shown in the overview of the model in orange in the main picture.
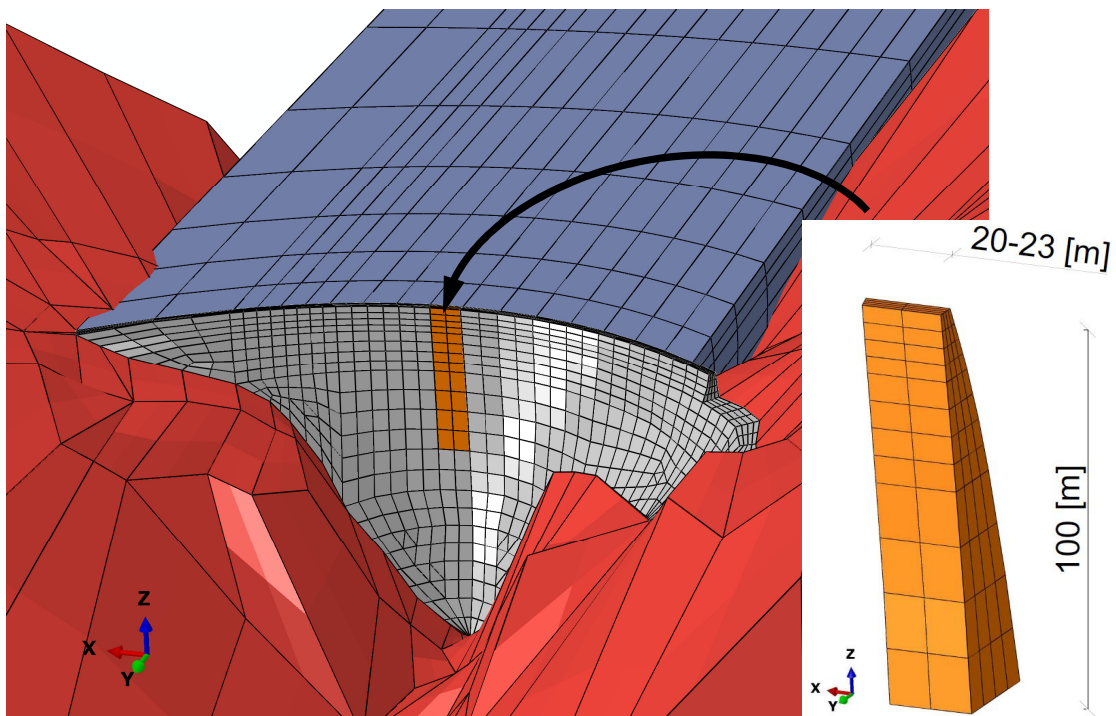

Figure 5-3   Dimension of the model block with its location in the arch dam

5.1.4   Element types used for the calculation

In this chapter the element types of the defined parts, namely the dam and a single model block, the foundation and the water are described.

The elements which are chosen for the calculation in this thesis are shown in the following picture. The element type used for the calculation of the arch dam behaviour and the behaviour of the model block is the element with the linear shape function (Figure 5-4 left side) and is named C3D8R. In this name C means that the used elements are continuum elements. All calculations in this thesis are 3 dimensional. Because of that there is a 3 and a D in the second and third place of the names. The 8 stands for the number of element nodes of a linear hexagonal element (next picture on the left). The R indicates the applied reduced integration which prevents shear locking in case of bending. The reduced integration can be applied because of the relative small displacements of the arch dam.

The foundation element type is a C3D20R element (Figure 5-4 left side). This one is a 20-nodes quadratic hexagonal element calculated with reduced integration - exactly the same as described for the arch dam above.
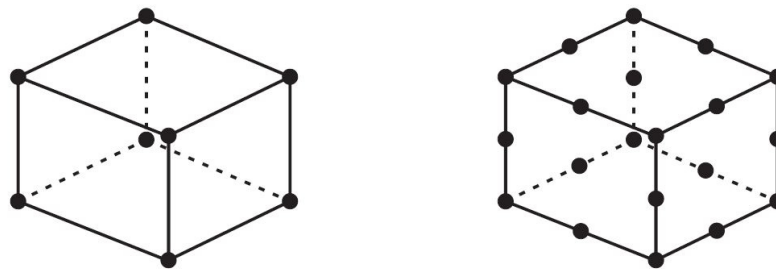

Figure 5-4   Hexagonal linear (left) and quadratic (right) finite element (source: [11])

The element type of the water is an AC3D20R. In comparison to the element for the foundation the A at the beginning of the name accounts for acoustic elements. Because of the dynamic earthquake calculation and the influence of the water on the arch dam this elements have to be defined as mentioned in the previous sentence. These elements are provided by the used program Abaqus to simulate the effects of fluids. The choice of the water elements has to be seen in combination with the non-reflecting boundary condition of the storage end (Figure 5-5) explained in chapter 5.2.1.

5.2   Boundary conditions and interactions between the parts

5.2.1   Consideration of the non-reflecting property of the storage

During an earthquake respectively the dynamic action the water in the storage absorbs the acoustic waves. Because of its mass the water in the storage cannot be stimulated and therefore the water has a dampening effect. To get calculation results which allow to assess the real dam behaviour this effect has to be considered in the defined numerical model.

In the subsequent picture you can see the backside (highlighted in yellow) of the modelled water. To model the acoustic impedance this backside is defined as a non-reflecting surface. This means that the reflections are numerically reduced to a minimum. The acoustic impedance of the reservoir´s side faces respectively the bottom face isn´t taken into account for the calculations of this thesis. This non-consideration leads to conservative calculation results and therefore to a safety puffer.
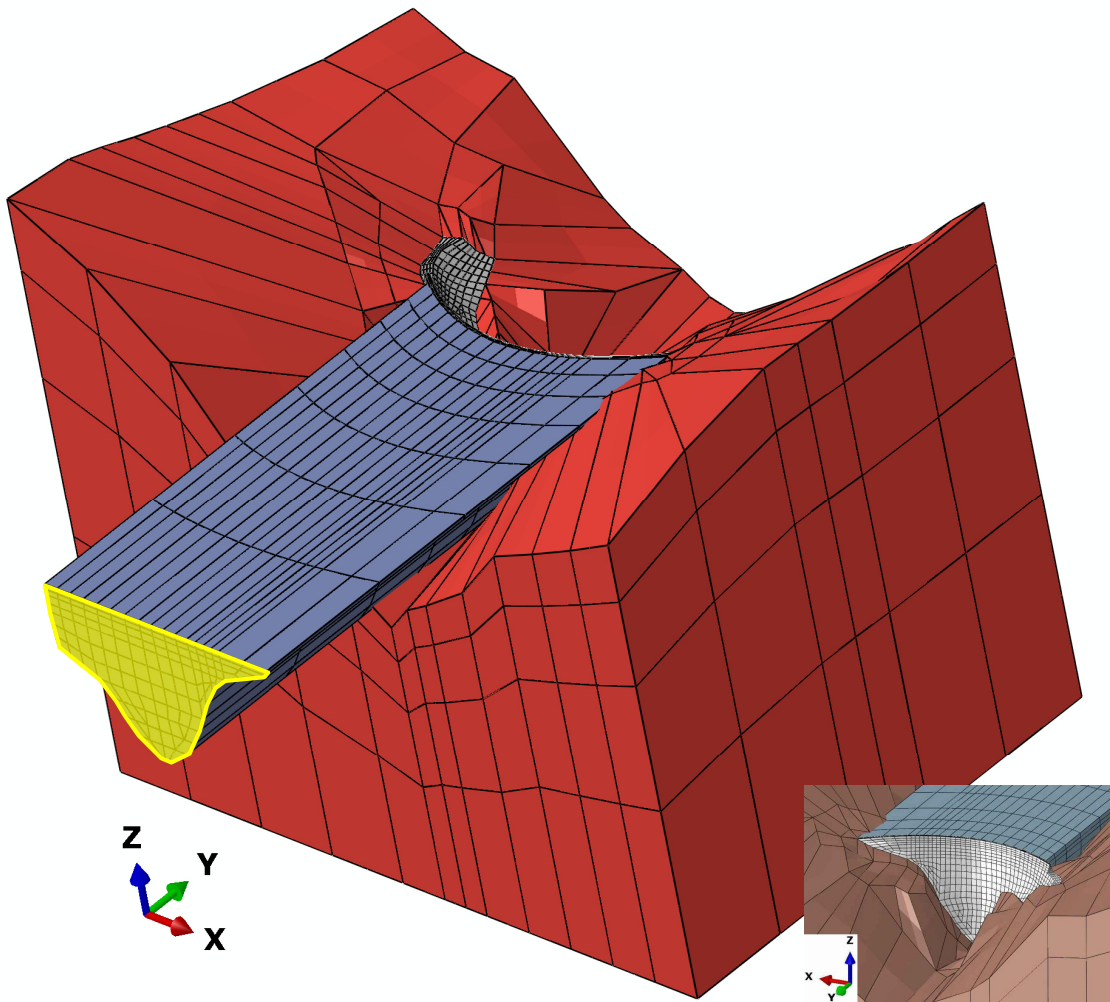

Figure 5-5   Backside of the modelled water

5.2.2 Consideration of the interaction in the joint between the arch dam wall and the defined block

For the interaction of the arch dam and the defined block (chapter 5.1.3) only two properties are defined. For the tangential behaviour (relative motion in direction of the flow) between the two joint faces a friction angle of 30° is introduced in the numerical model. The normal behaviour of the two contact faces is defined as "hard contact". "Hard contact" means, that the penetration between the two parts (dam and block) is minimized and also the transmission of tensile stresses between the contact faces isn't possible. The effect of shear keys is not defined. This leads to an underestimation of the factor of safety.

5.2.3 Consideration of the viscous damping

For the dynamic calculations the values of the viscous damping are defined with a magnitude of 0,6 for α and 0,001 for β. These values are given by the formulators of the benchmark workshop. The theoretical background of this values is explained in chapter 3.3.3.

5.3 Characteristic of the defined materials of the numerical model

The following chapters describe the defined materials and their consideration in the used finite element model.

5.3.1 Consideration of the foundation on rock in the numerical model

The picture below shows the foundation of the numerical model. For a better orientation the right side of the picture shows the whole numerical model with its three different parts. These are the foundation (brown), water (light blue) and the concrete dam (grey). The purple area on the left side shows the contact face of the double curved arch dam and the foundation. The foundation which is taken into account is 1020 [m] long, 760 [m] wide and has a minimal height on the arch dam foot of 435 [m] (see right picture).
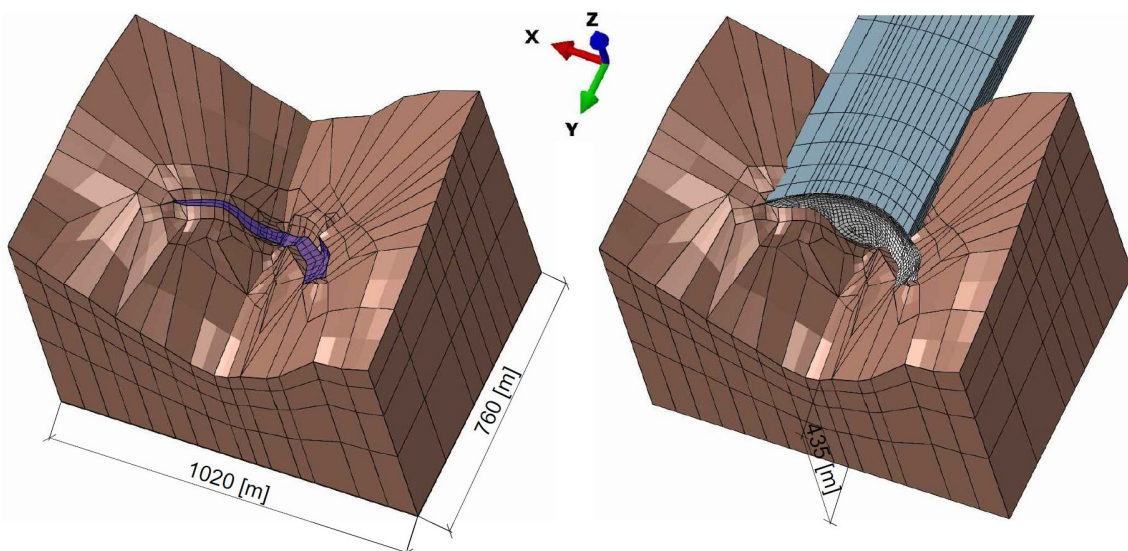

Figure 5-6   Dimensions of the considered rock foundation

The used property values for the foundation (rock) which are introduced into the numerical program are listed below. The first two rows are the moduli of elasticity and are divided in one for the static calculation and one for the dynamic calculation (earthquake). The last row contains the Poisson´s Ratio which doesn´t distinguish between dynamic and static calculations.

Mass Rock Properties	Unit	Value
Static Modulus of Elasticity, E_s	GPa	18.6
Dynamic Modulus of Elasticity, $E_d = 1.25 \cdot E_s$	GPa	23.3
Poisson's Ratio, v	-	0.20

Table 5-1　　　　　Material properties of the considered rock foundation (source: [4])

5.3.2　Concretes used for the modelled double curved arch dam

Regarding the concrete it has to be said that there are differences between the old concrete which was used from 1958 to 1963 to build the water retention structure (Luzzone dam) up to a height of 208 [m] and the newer one. The properties of the newer one which was used in the year 1996 to raise the dam about 17 [m] to a total height of 225 [m] are worse. In the figure below the newer concrete is pictured in pink and the older one in grey. In the right corner on the bottom of the picture is a figure of the assembly for a better orientation.
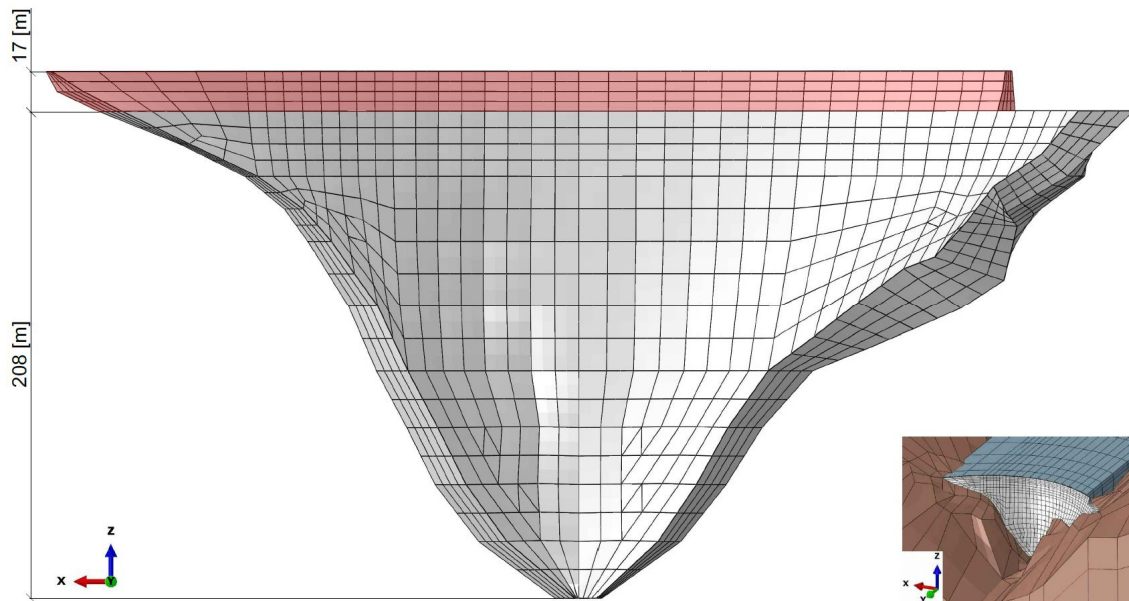

Figure 5-7　　　　　Demarcation of the old concrete and the newer one

The list below contains the values of the two used concretes. As previously said, Figure 5-7 shows the areas where the different concretes are applied. Similar to chapter 5.3.1 it has to be differentiated between the properties of the static calculation (highlighted in red) and the dynamic calculation (highlighted in blue). The general properties are highlighted in white.

Mass Concrete Properties	Unit	Value	
		Old Concrete	New Concrete
Density, ρ	t/m^3	2.5	2.4
Static Modulus of Elasticity, E_s	GPa	20	18
Dynamic Modulus of Elasticity, $E_d = 1.25 \cdot E_s$	GPa	25	22.5
Poisson's Ratio, ν	-	0.18	0.18
Thermal expansion, α	1/°C	10^{-5}	10^{-5}
Static Compressive Strength, f_c	MPa	38	32
Dynamic Compressive Strength, $f_{cd} = 1.5 \, f_c$	MPa	57	48
Static Tensile Strength, f_t	MPa	3	2.3
Dynamic Tensile Strength, $f_{td} = 1.5 \, f_t \leq 4 \, MPa$	MPa	4	3.5

Figure 5-8   Material properties of the dam concretes at different loads (dynamic → blue; static → red) (source: [4])

5.3.3   Water-characteristic-data used for the reservoir

In contrast to the material data of the concrete and the rock the characteristic data of the water is identical for the static calculation and the dynamic calculation. Because of the identity of the characteristic data for the static and dynamic calculation only two input values are necessary. These two values are the density ρ with a magnitude of 1000 [kg/m³] and the bulk modulus with a magnitude of 2073,6 [MPa].

5.4 Considered static loads

5.4.1 Consideration of the self-weight of the double curved arch dam

Because of the gravitation the self-weight and the water pressure (chapter 5.4.2) are the main static loads which are considered in the present thesis. The acceleration due to the gravity is considered with g= -9,81 [m/s²]. The negative acceleration value is a result of the orientation of the coordinate system of the numerical model. The gravity acts in the opposite direction of the z-axis of the coordinate system and therefore the according value has to be treated as negative (see the overview picture on the lower left side of Figure 5-9 shows the fact why the gravity has to be respected negative. In addition to the gravity also the mass of the calculated body has to be known. The self-weight of any part can be calculated as follows:

$$F_i = m * g \qquad [MN] \qquad (5\text{-}1)$$

To calculate the mass of the modelled arch dam the mass of the whole dam has to be known.

Figure 5-9 displays the way how the used finite element program calculates the dam´s self-weight. The self-weight-loads of the single dam elements are added up to a total self-weight load which´s formula is written below:

$$F_{Ges} = \sum_{i=1}^{n} F_i \qquad [MN] \qquad (5\text{-}2)$$

In the subsequent picture the red arrows (oriented in negative z-direction) on the green coloured wall and the related green coloured modelled-block show the loading due to the gravity. Every arrow stands for the gravitational load of one element (formula (5-1)). As mentioned above the total self-weight of the double curved arch dam is the sum of the self-weights of all elements and can be calculated with formula (5-2).

During the construction phase initial stresses due to the gravity occur. Displacements would also occur but they are compensated during the construction phase and therefore there are no displacements after completion. The fact of the compensation is considered in Abaqus in the step module with a special implementation by means of a geostatic step-type.
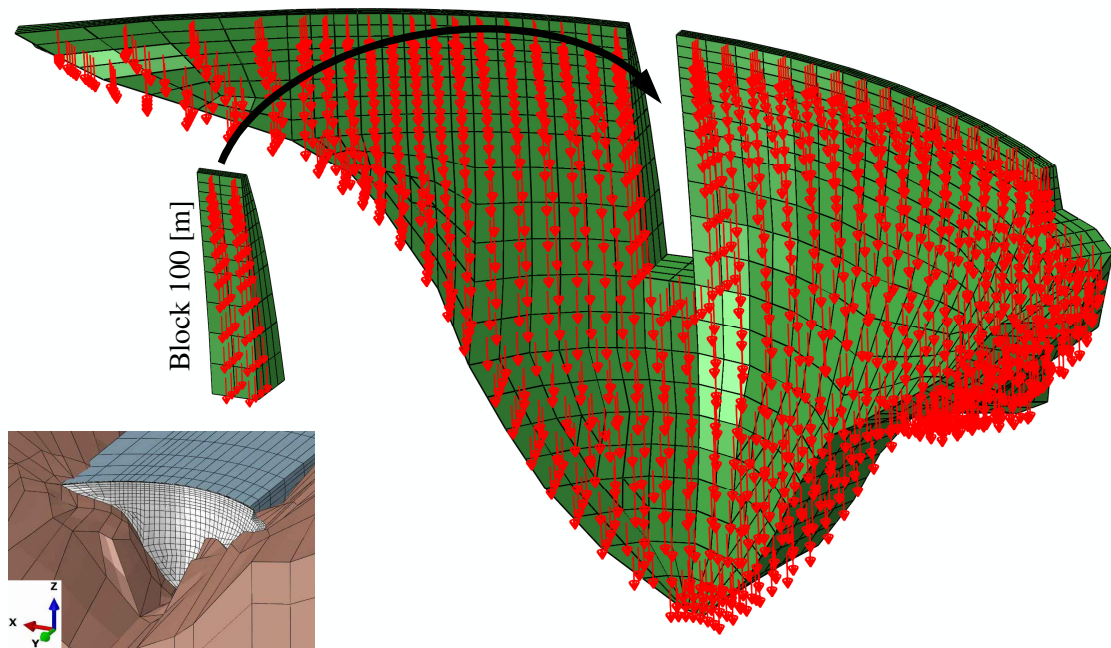
Figure 5-9   Consideration of the gravity in the used finite element model

5.4.2   Consideration of the hydrostatic load

As already mentioned in chapter 5.4.1 the water pressure is in addition to the self-weight the second main static loading of the double curved arch dam. The water pressure is acting hydrostatic on the dam (blue triangle in Figure 5-10). The maximum magnitude which occurs at the dam foot is calculated as follows:

$$p = \gamma_{water} * h \qquad \text{[MPa]} \qquad (5\text{-}3)$$

The next picture (Figure 5-10) shows the distribution of the water pressure (highlighted in blue) at the arch dam. The figure depicts the upstream face of the wall. On the red coloured area of the shown face the water pressure acts. The green dam area indicates the face which touches the rock where no water pressure occurs.

The coordinate system on the bottom left in combination with the overview on the bottom right picture side show the orientation of the red face. The total height of the water surface (zero water pressure) is defined in the instructions with 1606 [m.a.s.l.]. Because of this condition and the relative water height of 221 [m] the maximum water pressure magnitude at the dam foot was defined with 2,21 [MPa].
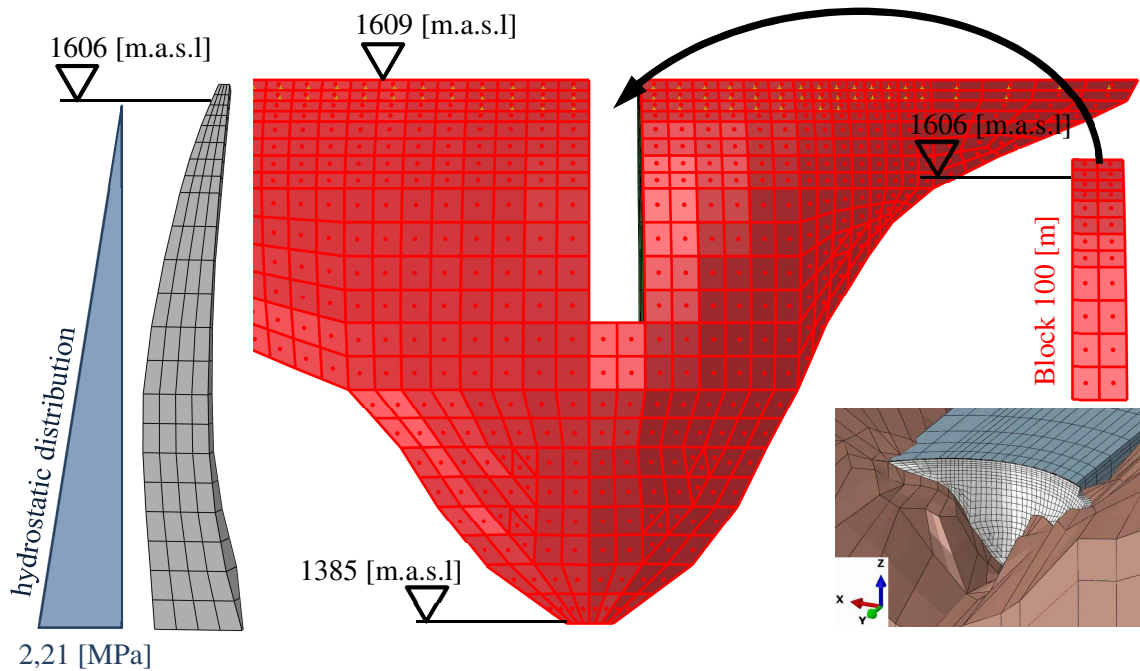
1606 [m.a.s.l]

1609 [m.a.s.l]

1606 [m.a.s.l]

Block 100 [m]

hydrostatic distribution

1385 [m.a.s.l]

2,21 [MPa]

Figure 5-10   Area of the acting of hydrostatic pressure

5.4.3   Consideration of the silt-load

Suspended particles and solids are deposited in the reservoir. The velocity of the water upstream from the retention structure which fills the storage is higher than at the wall where the velocity is zero. This means that the suspended particles and solids are transported till the wall. And because of the zero velocity at the wall the sedimentation starts. This effect is considered with an area load which's distribution is hydrostatic but due to the density of the sediments with a higher magnitude than in chapter 5.4.2.

The following Figure 5-11 shows the upstream side of the double curved arch dam. The area highlighted in red is the region where the silt load occurs. The picture on the bottom right side in Figure 5-11 in combination with the coloured arch dam wall shows that the sedimentation takes place on the water side of the dam. You can also see that the silt surface is at 1440 [m.a.s.l.]. The height of the silt is 55 [m].

The silt pressure is defined by the formulators of the benchmark workshop with the mass m= 400 [kg/m³] [4]. In combination with the gravity, the relative silt height and formula (5-4) the silt pressure is 0,216 [MPa].

$$p = m * g * h \qquad [\text{MPa}] \qquad (5\text{-}4)$$

The distribution of the silt pressure is visualised in Figure 5-11.
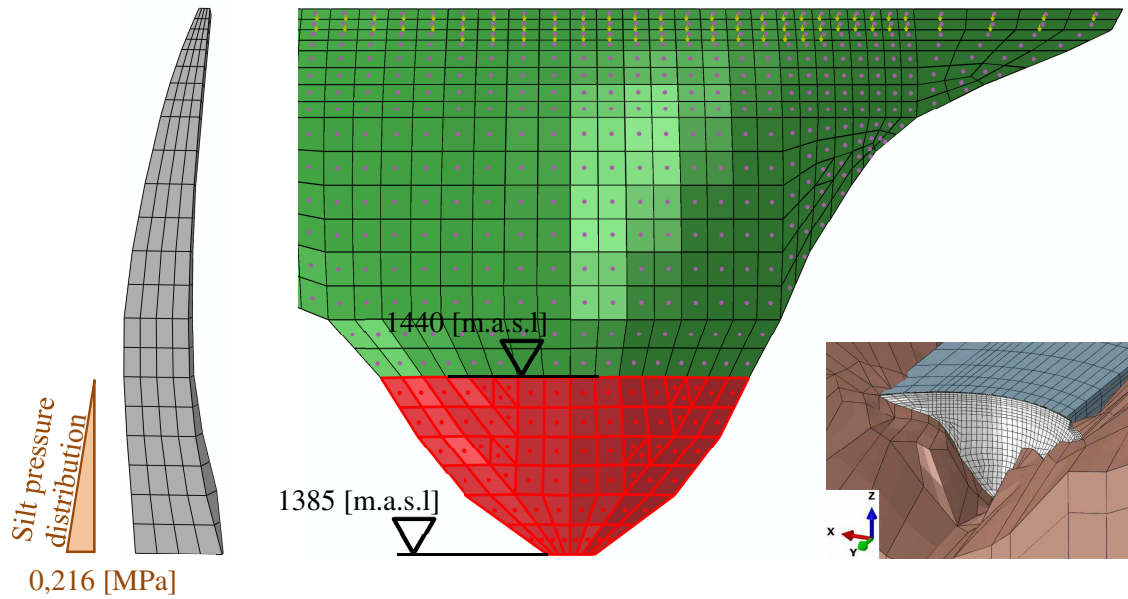
Figure 5-11   Consideration of the sedimentation in the finite element model in form of an silt load

5.4.4   Consideration of the temperature load

The following representation shows the annual temperature variation for the upstream face on the left side of the cross section (middle) and the annual temperature for the downstream face on the right side of the cross section. The temperature written on the abscissa in combination with the dam height (ordinate) gives the depicted thermal gradient. The blue lines show the winter temperature, the red lines the summer temperature and the green lines represent the average temperature in summer and winter. For the basic model (chapter 5.1.1) the temperature of the single nodes are given.
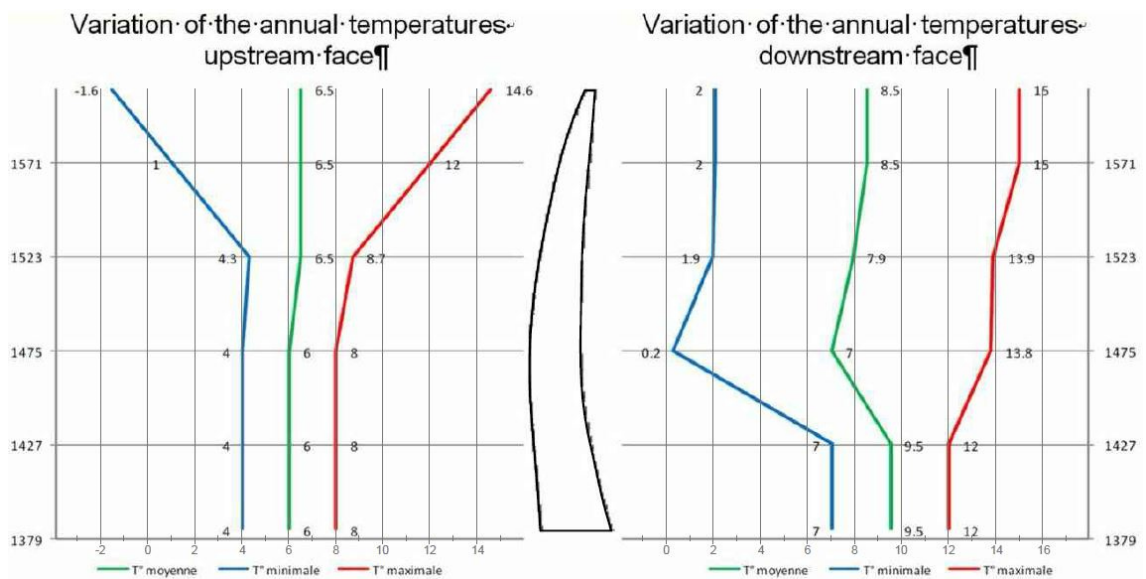
Figure 5-12   Variation of the annual temperatures for winter, summer, upstream- and downstream face (source: [4])
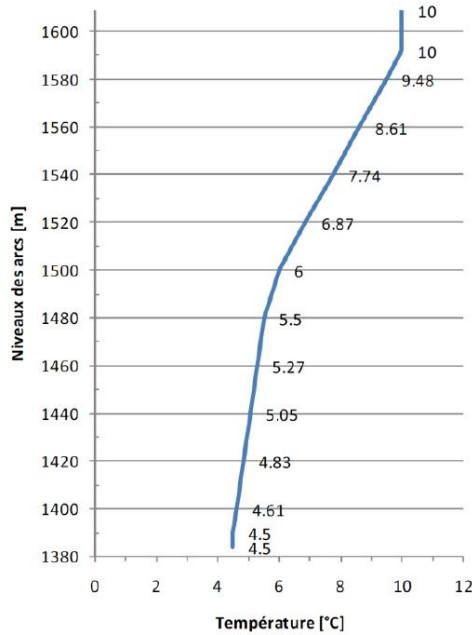
Figure 5-13   Grouting temperature-distribution (source: [4])

Because of the refined mesh of the dam of the used FE-model (chapter 5.1.2) the temperature loading has to be defined. For the basic model the temperature loading is given.

The adjacent figure shows the dam body temperature at grouting time. Like in Figure 5-12 in Figure 5-13 the temperature is also written on the abscissa and the height on the ordinate. The combination of the temperature and the height gives the drawn thermal gradient (blue).

To get the necessary temperature field for the calculation the relative temperature has to be calculated. Therefore the temperature at grouting time has to be subtracted from the temperatures in Figure 5-12 (formula (5-5)). This means that the arch dam isn´t affected by the grouting temperature distribution and is only loaded due to the temperature difference between the grouting temperature and the annual temperatures.

For the upstream face which touches the rock, a constant temperature field with 10°C for the summer load respectively 3°C for the winter load is used. For the input into the FE-model also for the upstream face the temperature relative to the temperature at grouting time has to be calculated.

The considered additional temperature loading is calculated as follows:

$$\Delta t = t_{annual} - t_{grouting} \qquad [°C] \qquad\qquad (5\text{-}5)$$

5.5 Seismic data used for the FE-calculation

5.5.1 Earthquake acceleration used for the calculation

Figure 5-14 shows a detail of the earthquake intensity map of Switzerland. For the calculation of the peak ground acceleration which acts in the area of the arch dam, the earthquake intensity (MSK-scale) based on the following map has to be known. For the Luzzone Dam this MSK-intensity (Medwedew-Sponheuer-Karnik-intensity) is approximately 7,7
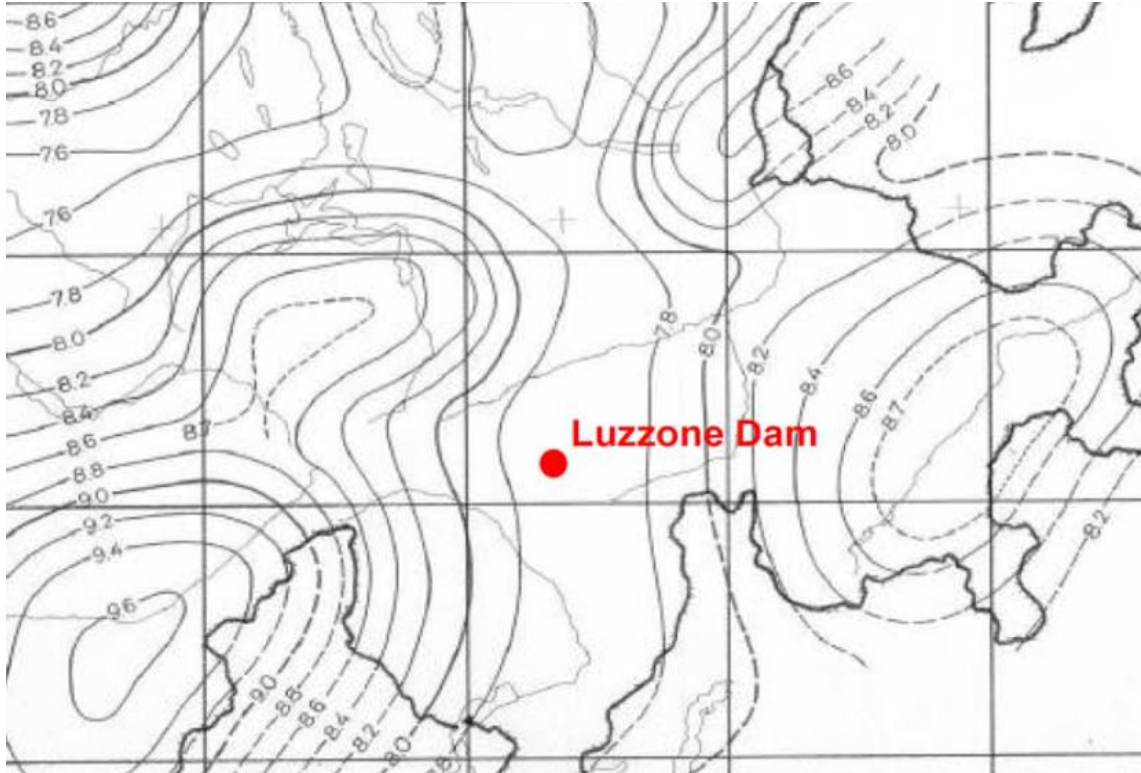

Figure 5-14   Detail of the earthquake intensity map (MSK scale) for Switzerland for the location of the dam (source: [4])

After determining the MSK-value the horizontal and vertical peak ground acceleration can be calculated. The subsequent steps respectively formulas show this calculation (source: [4]).

$$\log a_h = 0{,}26 * l_{MSK} + 0{,}19 = [\frac{cm}{s^2}] \tag{5-6}$$

$$a_h = 1{,}57 \left[\frac{m}{s^2}\right] = 0{,}16 \ g \tag{5-7}$$

The mainly used acceleration values in this thesis are 1,57, 3,14 and 4,71 [m/s²]. To get a better impression of the dam behaviour also 6,28 [m/s²] is used once (chapter 6.5.2.).

The vertical acceleration is 2/3 of the horizontal acceleration (a_h) and calculated as follows (source: [4]):

$$a_v = \frac{2}{3} * a_h = \frac{2}{3} * 1{,}57 = 1{,}04 \left[\frac{m}{s^2}\right] = 0{,}106 \, g \tag{5-8}$$

5.5.2 Consideration of the acceleration time history

To assess the non-linear behaviour of an arch dam during an earthquake, time histories of the earthquake event are needed. Every direction of an arch dam's coordinate system (for example the coloured arrows in Figure 5-5) has its own time history.

The data provided by the formulators of the benchmark workshop contains three series of time histories. Each series contains time histories for the X-, Y- and Z-direction. For the present thesis only one of the three series containing time histories for the X-, Y- and Z-directions is used for the calculations.

The following picture shows exemplarily the used time history of the X-direction:
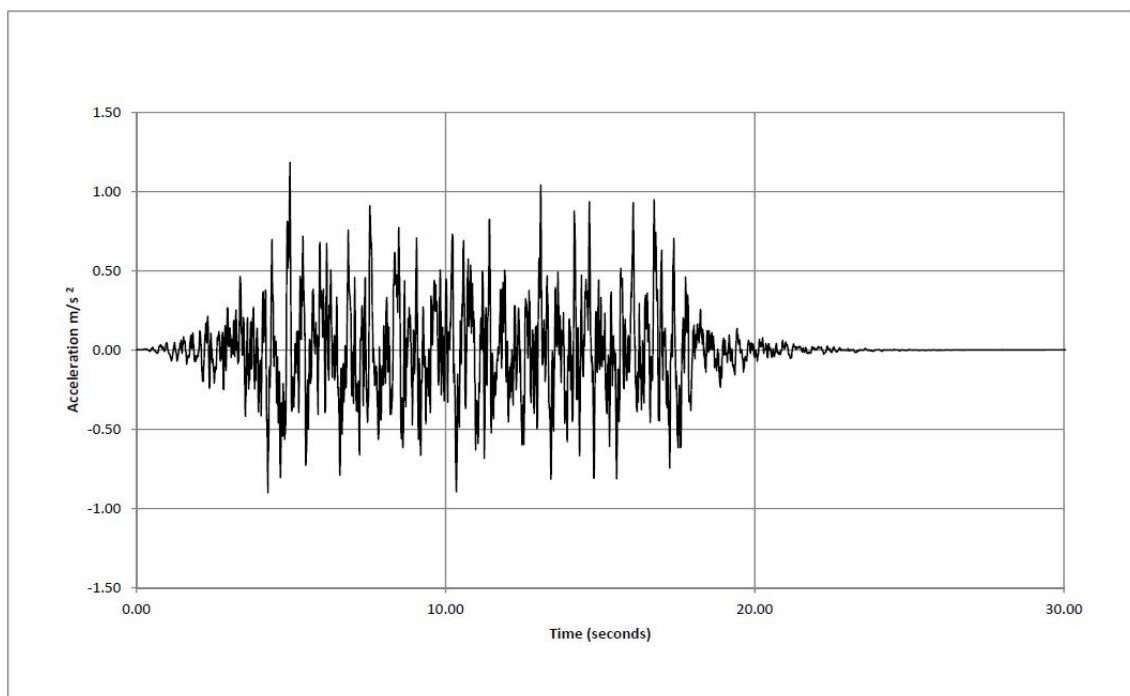
Figure 5-15   Acceleration time history in X-direction (source: [4])

6 Analysis results

6.1 Load combinations used for the evaluations

The following two tables show the load combinations used for the evaluations in this chapter.

Load combinations of the following results		
Considered load	Static calculations	
	Chapter 6.2 Comparison FE- and analytical calc.	Static displacement gradient
Self-weight	-	✓
Water pressure	✓	✓
Silt load	-	✓
Temperature load	-	✓
Earthquake acceleration	-	-

Table 6-1   Static load combinations for the calculations

Load combinations of the following results			
Considered load	Dynamic calculations		
	Chapter 6.5 Displacments due to earthquake	**Chapter 6.6** Analysing of the block joints	**Chapter 6.7** Acceleration on the dam crest
Self-weight	✓	✓	✓
Water pressure	✓	✓	✓
Silt load	✓	✓	✓
Temperature load	✓	✓	✓
Earthquake acceleration	✓	✓	✓

Table 6-2   Dynamic load combinations for the calculations

6.2 Comparison of evaluations for plausibility check

6.2.1 Calculation with the pipe formula

The following formulas are the basis for the calculated evaluations which are shown in Figure 6-2 (grey). First of all the hydrostatic pressure p has to be calculated (specific weight times water depth). In the next step this value is used to calculate the hoop stresses at different depths. In formula (6-2) you can see that also a radius and a thickness are necessary for this calculation.

$$p = \gamma * t \qquad \text{[MPa]} \qquad (6\text{-}1)$$

$$\sigma_{11} = \frac{p * r}{s} \qquad \text{[MPa]} \qquad (6\text{-}2)$$
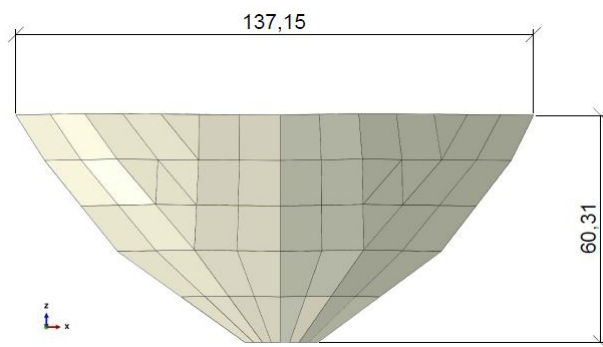
Table 6-3 shows the calculated hoop stresses σ_{11} at different water depths. All radiuses in Table 6-3 are measured results for the curvature of the double curved arch dam from pictures which are inserted into AutoCAD (for example Figure 6-1). The thickness of the arch dam is also a measured value from this pictures.
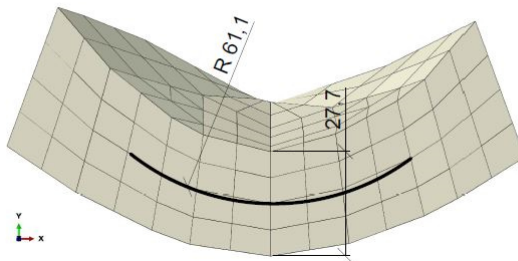
Figure 6-1   Radius for calculation (for example at t = 160,69 [m])

h [m]	t [m]	g [m/s²]	γ [kN/m³]	p [MPa]	r [m]	s [m]	σ_{11} [MPa]
200.090	20.91	9.81	9.81	0.205	244.62	11.69	-4.292
165.580	55.42	9.81	9.81	0.544	183.33	18.08	-5.513
110.280	110.72	9.81	9.81	1.086	109.57	25.14	-4.734
60.310	160.69	9.81	9.81	1.576	61.10	27.70	-3.477
24.120	196.88	9.81	9.81	1.931	35.19	30.90	-2.200

Table 6-3   Calculation of hoop stresses with pipe formula

6.2.2   Diagram for comparison of FE-and pipe formula calculation

The following diagram, which displays a comparison between the FE-calculations and an analytical calculation with the pipe formula (described in section 6.2.1) also shows a sketch for better orientation (left side). The abscissa of the diagram shows the hoop stresses of the double curved arch dam and the ordinate the dam height. As you can see in the legend the values of the grey line are calculated with the mentioned pipe formula. All other colored lines are evaluations of the FE-calculation. Orange stands for the evaluation of the upstream side of the pictured cross-section, red shows the evaluation at the middle and the yellow line is the evaluation result of the airside of the cross-section.

The comparison between the results of the two calculation methods shows a good accordance at the middle line of the cross-section (red line in the sketch). The approximated circular arc segment with its measured radius is also drawn in this middle line of the cross-section (for instance black curved line in Figure 6-1).
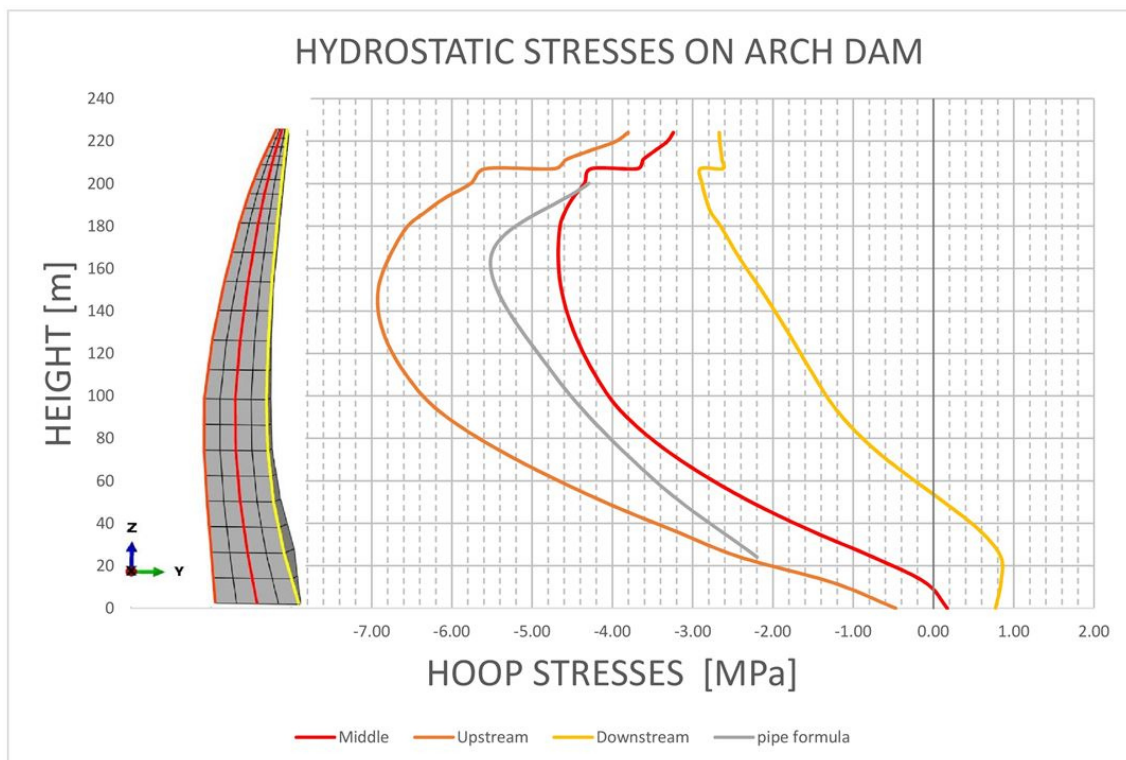
Figure 6-2   Comparison of FE-calculation and analytical calculation

In general it can be said that the approximately (analytically) calculated results show a good accordance with the numerical generated evaluation results. Therefore the plausibility check is successful.

6.2.3 Comparison of the natural frequencies

The following table shows the comparison between the natural frequencies of the dam which are calculated in this thesis and the values of a publication [6]. The deviation between the compared values is negligible. Therefore the plausibility check is again successful.

Mode	Calculation at empty reservoir	Comparative value at empty reservoir [6]	Calculation at full reservoir	Comparative value at full reservoir [6]
	f [Hz]	f [Hz]	f [Hz]	f [Hz]
1	1,98	1,99	1,51	1,51
2	2,09	2,09	1,52	1,53
3	2,98	3,00	2,10	2,10
4	3,74	3,76	2,26	2,26
5	3,91	3,94	2,38	2,39
6	4,39	4,43	2,80	2,80

Table 6-4   Comparison of the natural frequencies of the dam for plausibility check

6.2.4 Comparison of the modes of frequencies for plausibility check

The following table compares the natural modes 1- 3 from the according frequencies of the two right columns in Table 6-2. As you can see in Table 6-5 the two modes pictured in row three are quite the same. In contrast the first two modes in the left column (calculated in this thesis) and the first two modes in the right column (Source: [6]) are mirror inverted. This fact has no negative influence on the plausibility check because the water retention structure swings, similar to the natural modes of an Euler buckling bar (same physical principle), in both directions. To get the same results one mode of each row has to be multiplied by -1. Therefor the natural modes could be seen as equal and the plausibility check as successful.
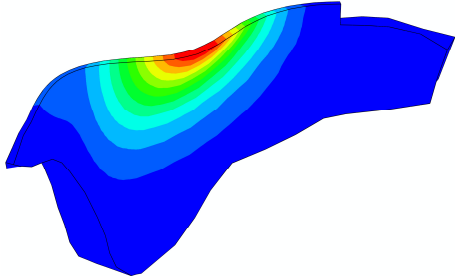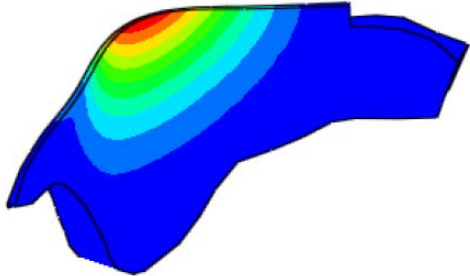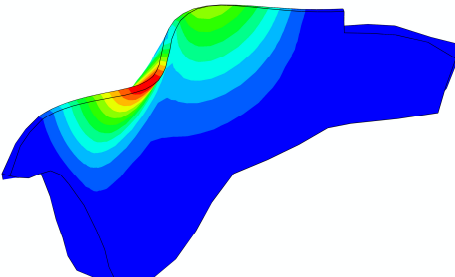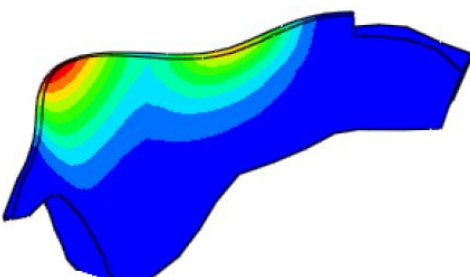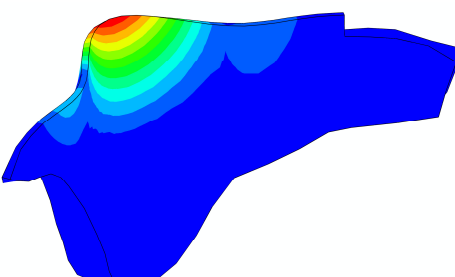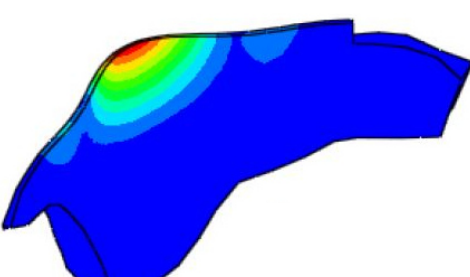
Mode Nr.	Calculated natural mode at full reservoir	Comparative natural mode at full reservoir [6]
1		
2		
3		

Table 6-5   Comparison between the calculated natural modes and natural modes of source [6] for plausibility check

6.3   Displacements due to earthquakes with different accelerations

6.3.1   Position of the evaluated displacements

The subsequent picture (Figure 6-3) shows the area where the different displacements are analysed. This zone is located at the middle cross section (red line) of the arch dam on the upstream face (blue dotted line). The following displacements which are shown in 6.3.2 and 6.3.3 are analysed along the blue dotted line.
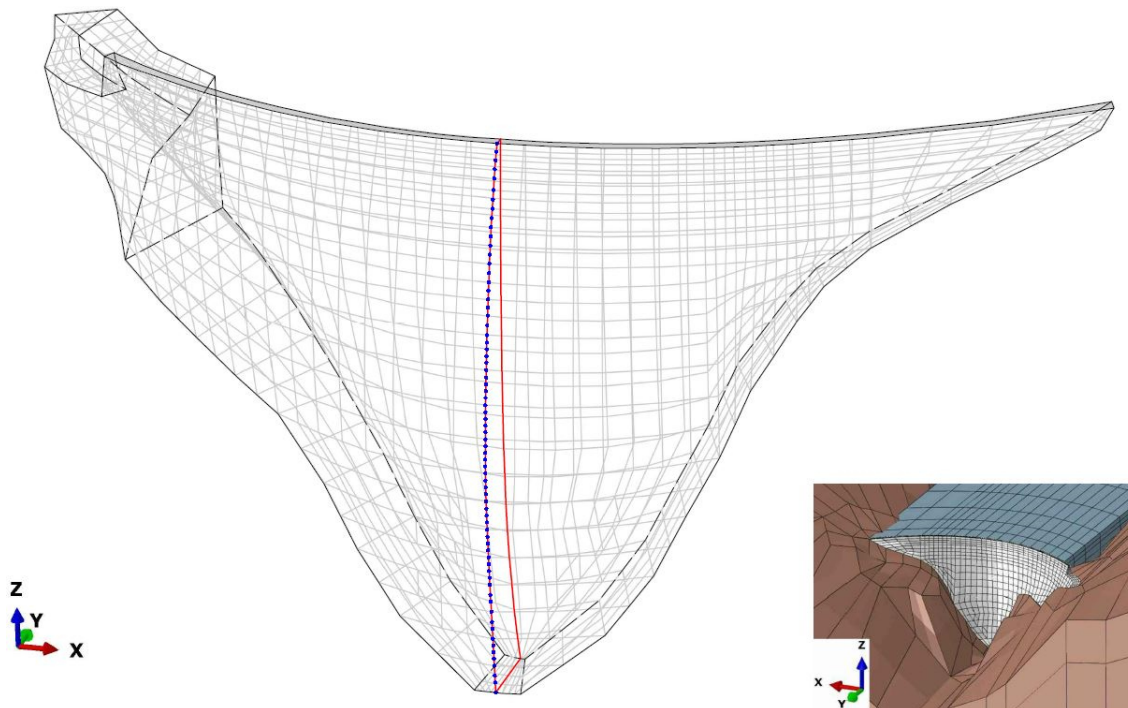
Figure 6-3   Area where the displacements are analysed

6.3.2 Comparison between the displacement values of a publication (source [6]) and the self-calculated computations

Figure 6-4 (source [6]) and Figure 6-5 (calculation for this thesis) show the relevant displacements for a plausibility check. The abscissa of both diagrams shows the moving in radial direction of the double curved arch dam at different heights (ordinate). The total height of the dam is 224 [m]. In both diagrams the middle line shows the static displacement, the right line the positive dynamic dam movement and the left line the negative dynamic dam movement. Both dynamic lines are calculated with an earthquake acceleration of a=1,57 [m/s²].

Figure 6-4   Radial displacement at middle cross-section in summer at an earthquake acceleration of a=1,57 [m/s²] (source: [6])

A comparison between the two pictures shows a small deviation of the results. The difference at the positive maximum movement (0,26 [m] in Figure 6-5 and 0,22 [m] in Figure 6-4) due to dynamic loading at the dam crest is 0,04 [m]. The difference at the negative dynamic movement is 0,077 [m] (0,087 in Figure 6-5 minus 0,01 [m] in Figure 6-4).

Investigations regarding the reason for the deviation show that only the consideration respectively the non-consideration of the acoustic impedance of the reservoir´s side faces and the bottom face are responsible for the difference. The difference of the mesh size of the used models has no noteworthy effect. Both diagrams of this subchapter are calculated with a time history (chapter 5.5.2) and an implicit calculation method.

Figure 6-5   Radial displacement at middle cross-section at an earthquake acceleration of a=1,57[m/s²] in summer

6.3.3 Displacement due to different earthquake accelerations and temperatures

The displacements are computed with different acceleration values (chapter 5.5.1) and a temperature loading (chapter 5.4.4) which simulates the influence of the summer (Figure 6-6) respectively the winter temperature (Figure 6-7). The principle of the diagrams is the same as in Figure 6-4 and Figure 6-5. The abscissa shows the radial displacement at the middle cross-section at the upstream face (red line in the sketch in Figure 6-6) and the ordinate shows the height of the dam. As you can see in the legends of the diagrams the lowest acceleration is defined with a=1,57 [m/s²] (blue; baseline value). The others are 2 times (a=3,14 [m/²], red) and 3 times (a=4,71 [m/s²], yellow) the baseline value. The green dot-dashed line represents the static displacement without any dynamic influence.

Starting from the green dot-dashed line the diagram shows the maximum (continuous lines) and minimum (dashed lines) displacements at each earthquake excitation. A closer look at the deflection values shows a linear increasing (maximum displacement) and linear decreasing (minimum displacement) of the moving at the used earthquake acceleration. Chapter 6.3.4 explains this effect more in detail.
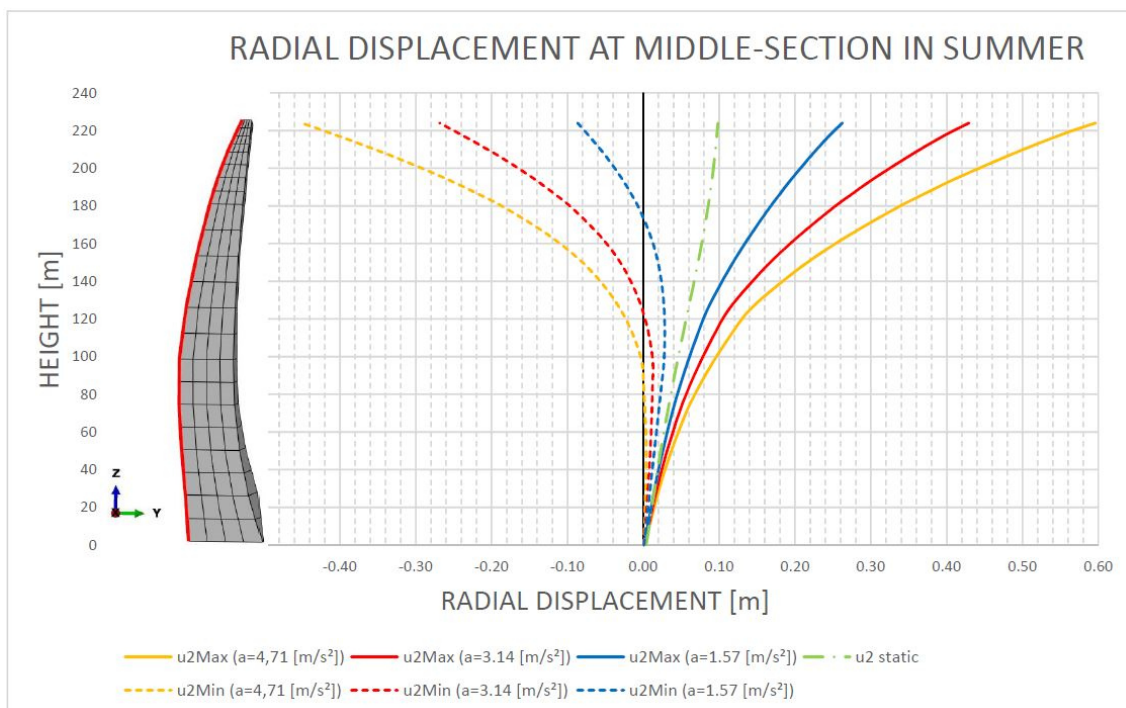
Figure 6-6　　　　Radial Displacements at middle cross section with different accelerations in summer
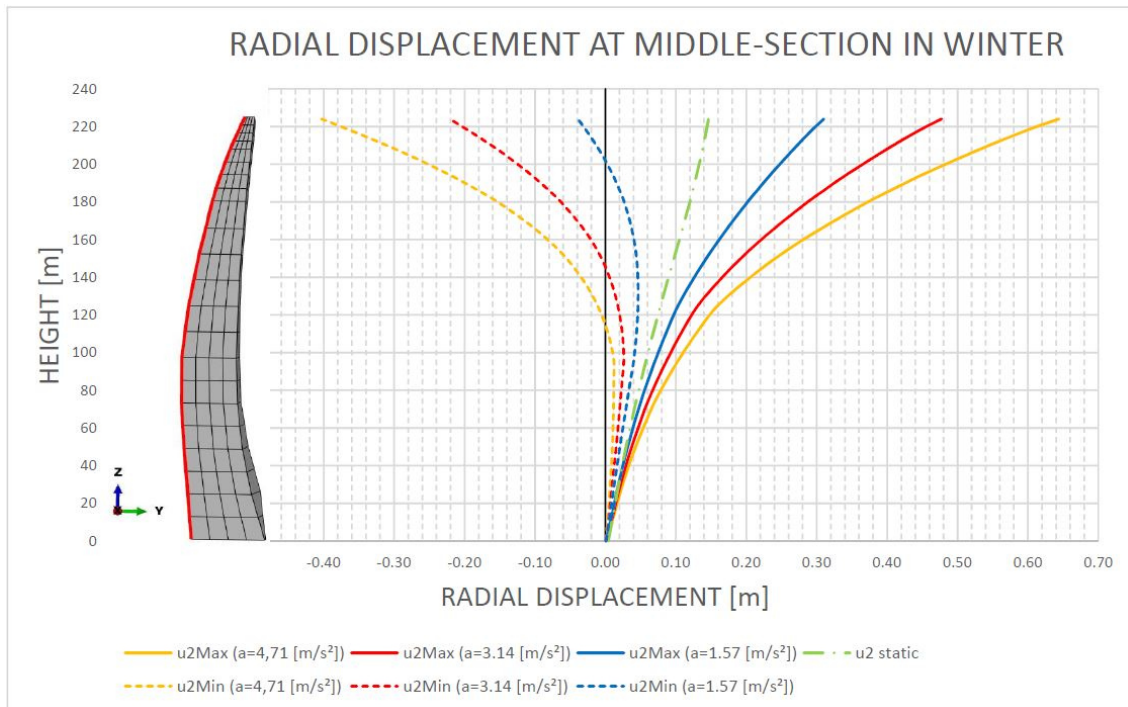
Figure 6-7   Radial Displacements at middle cross section with different accelerations in winter

6.3.4 Comparison of the displacement at the dam crest with different earthquake accelerations and temperatures

Table 6-6 summarises the maximum and minimum displacements at the dam crest described in the subchapters 6.3.2, 6.3.1 and 6.3.3. The detailed location of the evaluation point is shown in Figure 6-8 with the red point on top of the cross section in the sketch. The crest movements (u_2) in Table 6-6 at earthquake accelerations 1,57, 3,14 and 4,71 [m/s²] are also displayed in Figure 6-6 and Figure 6-7 at dam height 224 [m]. The other acceleration values (2,36, 3,93, 5,50 and 6,28 [m/s²]) of Table 6-6 are only calculated in this chapter as supporting points for the diagram. As you can see in the last two columns of the table the difference between the summer and winter temperature is always the same.

| Comparison of the radial displacement at the dam crown at diff. temp. | | | | | | | |
| Summer | | | Winter | | | Difference | |
a [m/s²]	$u_{2,max,sum,ti}$ [m]	$u_{2,min,sum,ti}$ [m]	a [m/s²]	$u_{2,max,win,ti}$ [m]	$u_{2,min,win,ti}$ [m]	$\Delta u_{2,max,sum/win}$ [m]	$\Delta u_{2,min,sum/win}$ [m]
1.57	0.262	-0.087	1.57	0.310	-0.039	0.048	0.048
2.36	0.346	-0.178	2.36	0.394	-0.130	0.048	0.048
3.14	0.429	-0.269	3.14	0.477	-0.221	0.048	0.048
3.93	0.513	-0.360	3.93	0.561	-0.312	0.048	0.048
4.71	0.596	-0.451	4.71	0.644	-0.403	0.048	0.048
5.50	0.680	-0.542	5.50	0.728	-0.495	0.048	0.048
6.28	0.763	-0.633	6.28	0.811	-0.585	0.048	0.048

Table 6-6   Comparison of the radial displacement at the dam crest at different temperatures

The following diagram is based on the depicted table above. The red coloured lines represent the evaluations of the calculations based on summer temperature and the blue coloured lines the evaluations of the calculations based on winter temperature. The continuous lines represent the maximum movements and the dashed lines represent the minimum movements of the dam crest.

The difference between the values of the calculation at summer temperature (red line) and the calculation at winter temperature (blue line) is always (at minimal and maximal displacement) the same. This fact is also shown in the last two columns of Table 6-6.
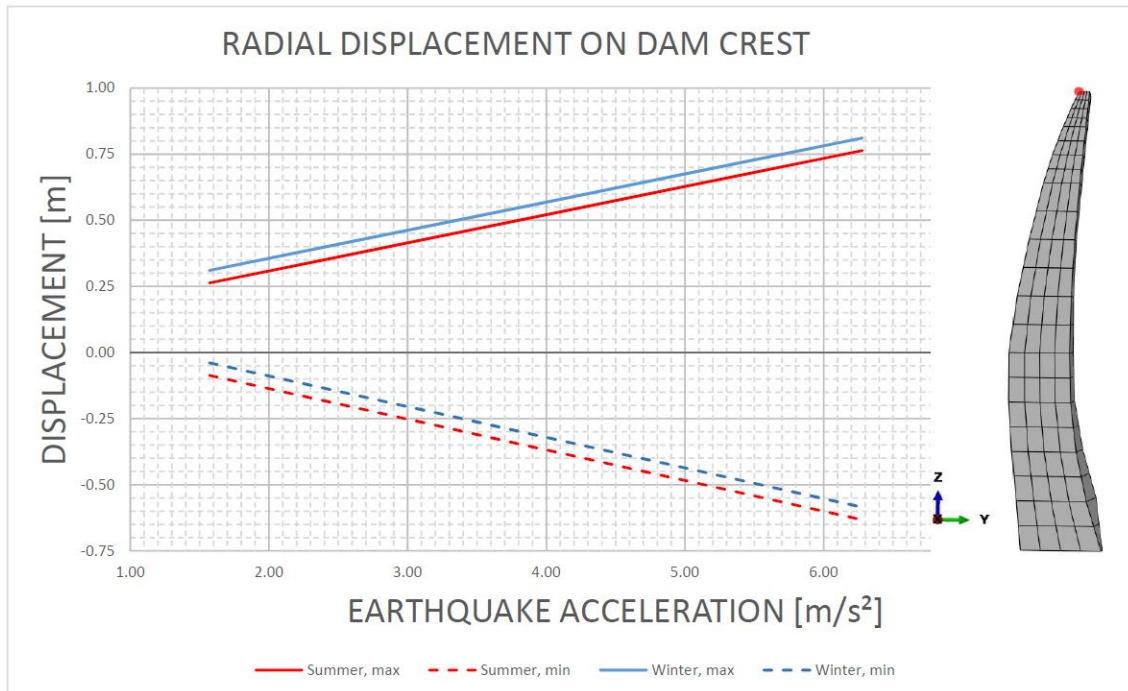
Figure 6-8   Radial displacement on the dam crest at middle cross section with different temperatures

6.4   Analysing of block joints at different earthquake accelerations

In this chapter the behaviour of the modelled block respectively the behaviour in the block-dam joint of the FE-model is analysed. The following subchapter defines the locations of the nodes used for the analysis. As mentioned in chapter 5.2.2 the effect of shear keys is not considered. Only a friction factor of 30° is defined and hard contact is assumed.

6.4.1   Locations of the block nodes where the post processing is done

The subsequent picture shows the locations where the following analyses are done. Node 7 and 27 are located in the upper area of the side face and node 155, 150, 11 and 35 are located in the lower area of the side face of the block. Those side nodes are pictured in blue. Nodes no. 195 and 189 are located on the block foot and are displayed in black.
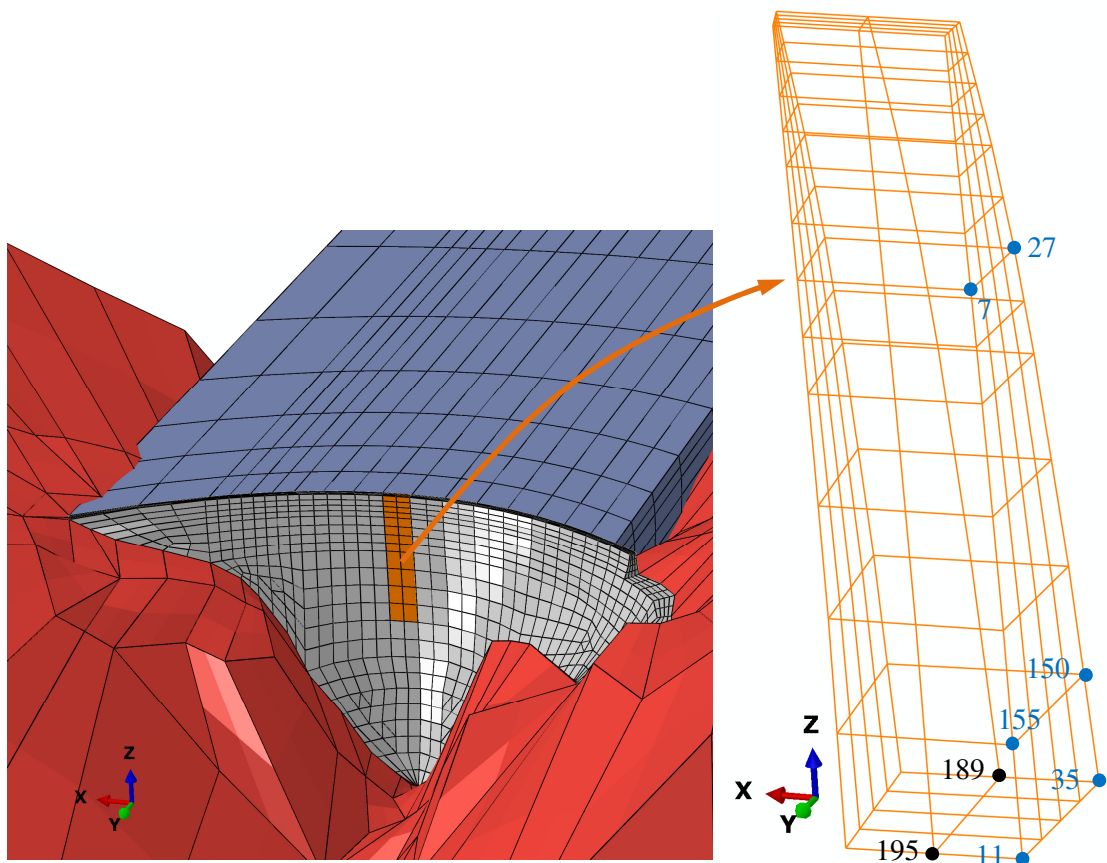
Figure 6-9   Locations of the block nodes where the analyses are done

6.4.2 Comparison of the joint opening and the corresponding contact pressure in winter for plausibility check

To insure that the present FE-model is correct also in this analysis chapter a plausibility check has to be performed like it is done in chapter 6.2 and 6.3.2. In the following diagram the joint opening (COPEN) and the contact pressure (CPRESS) at the selected evaluation point (block node 189) are compared. This evaluation is exemplarily chosen for an earthquake acceleration of a=3,14 [m/s²] and winter temperature.

On the abscissa of Figure 6-10 the time range of the earthquake (t=21÷26 [s]) for which this diagram is valid is written. There are two ordinates displayed. The left one shows the joint opening (COPEN) and is indicated in the diagram with the blue line. The right one displays the contact pressure (CPRESS) and is symbolized in the diagram with the orange line.

Subsequently you can see that at every joint opening (COPEN>0) the contact pressure is zero which is the consequence of the missing contact. The resulting interaction as shown in the diagram proofs that the plausibility check is successful.
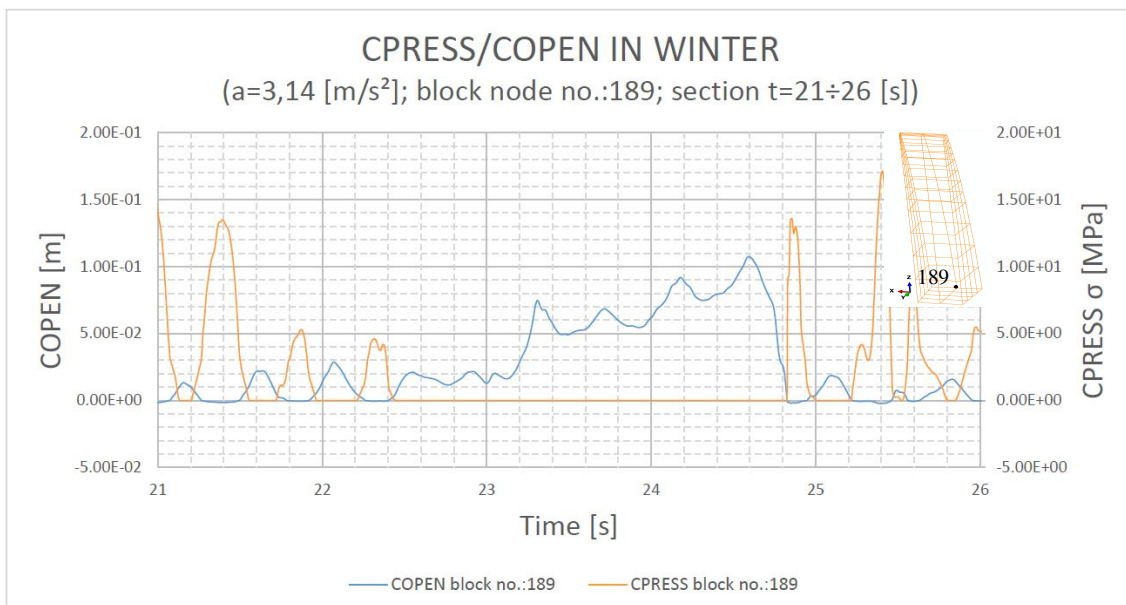
Figure 6-10   Comparison of the joint opening and contact pressure at block node 189

6.4.3   General explanations for the following diagrams Figure 6-11 to Figure 6-17

In the headline of each diagram the used earthquake acceleration and the numbers of the analysed nodes are specified. A sketch on the right side of the figure gives an overview of where the nodes are positioned at the block. The diagram is based on an earthquake duration of 30 seconds. The abscissa shows the relative time steps of the assumed earthquake. The ordinate (left or left and right side) shows the different evaluations of the joint (joint opening and relative motion of the contact faces). The coloured lines show the respective joint opening at the different time steps during the earthquake. Figure 6-17 depicts the joint opening as the sliding of the corresponding contact faces.

Except for Figure 6-17 every diagram compares an upstream and a downstream located node because at those two points the maximum difference is likely to show.

In addition the headline states the temperature loading (summer or winter) which was assumed for the FE-calculation. The legend on the bottom gives information about which colour is used for which node.

All diagrams are exemplarily chosen for calculations with different earthquake acceleration and temperatures (winter and summer).

6.4.4   Comparison of the selected block nodes at the block foot

The following two pictures display the comparison of the joint opening of node number 189 (upstream) and node number 195 (downstream) which locations are shown in Figure 6-9. The blue and red lines represent the joint opening (COPEN at the ordinate) of these nodes at the corresponding time step (abscissa). The underlying earthquake acceleration of this two diagrams is 4,71 [m/s²].

Subsequently you can see that the joint of the block foot stays open (coloured lines stay above the base line) after the earthquake loading. In both consecutive diagrams the joint opens at time step 16. After that the joint does not close again except at time step 24,5 for a short moment.
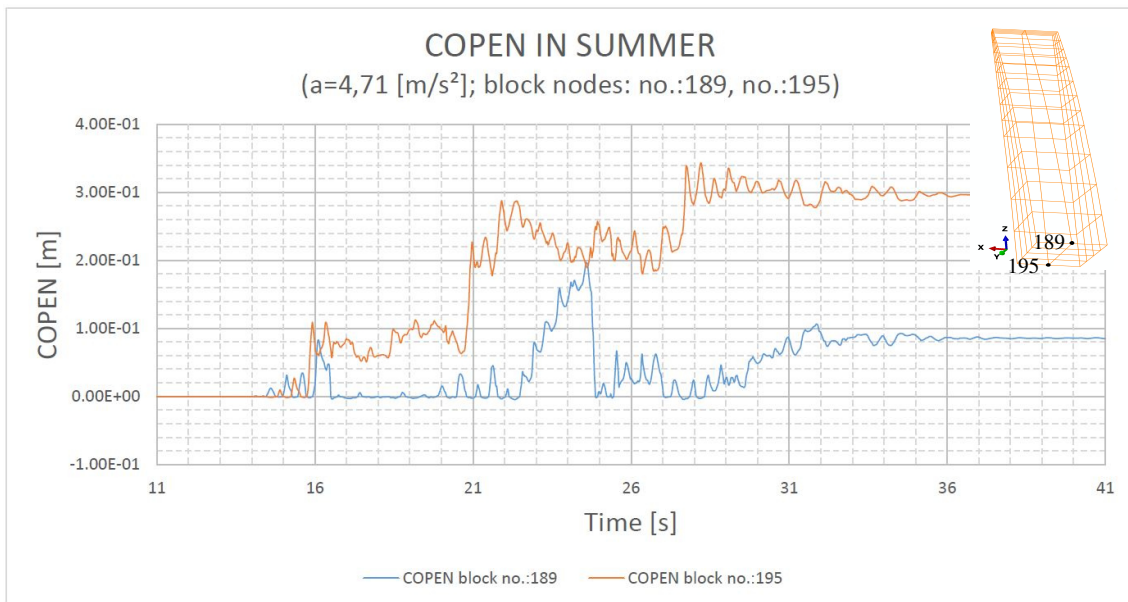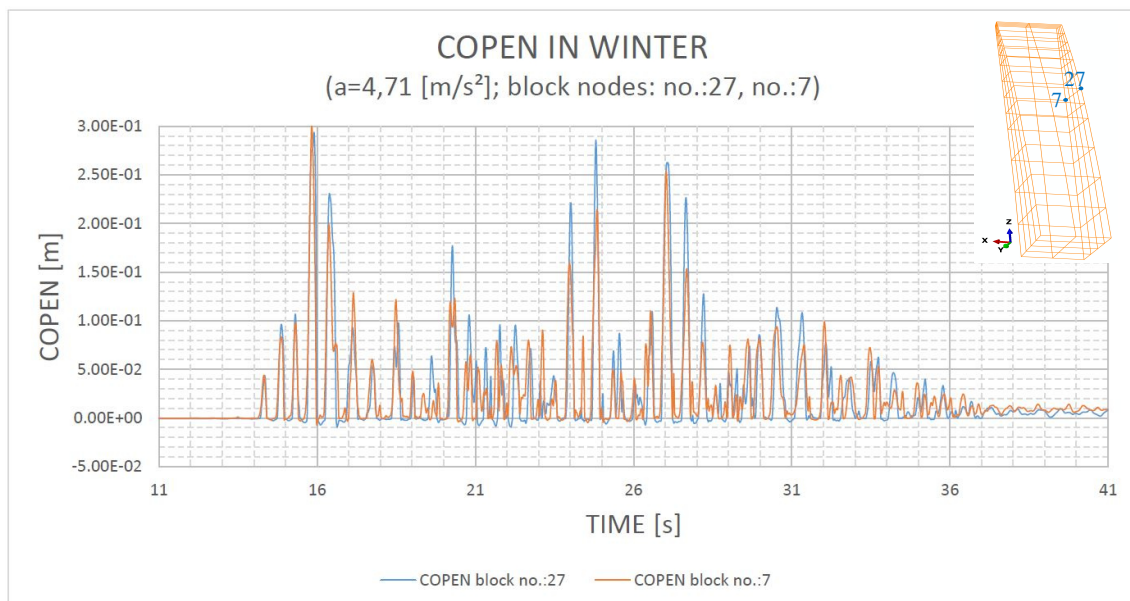
Figure 6-11   Comparison of the joint opening of block nodes 189 and 195 in summer (for example at earthquake acceleration a=4,71 [m/s²])
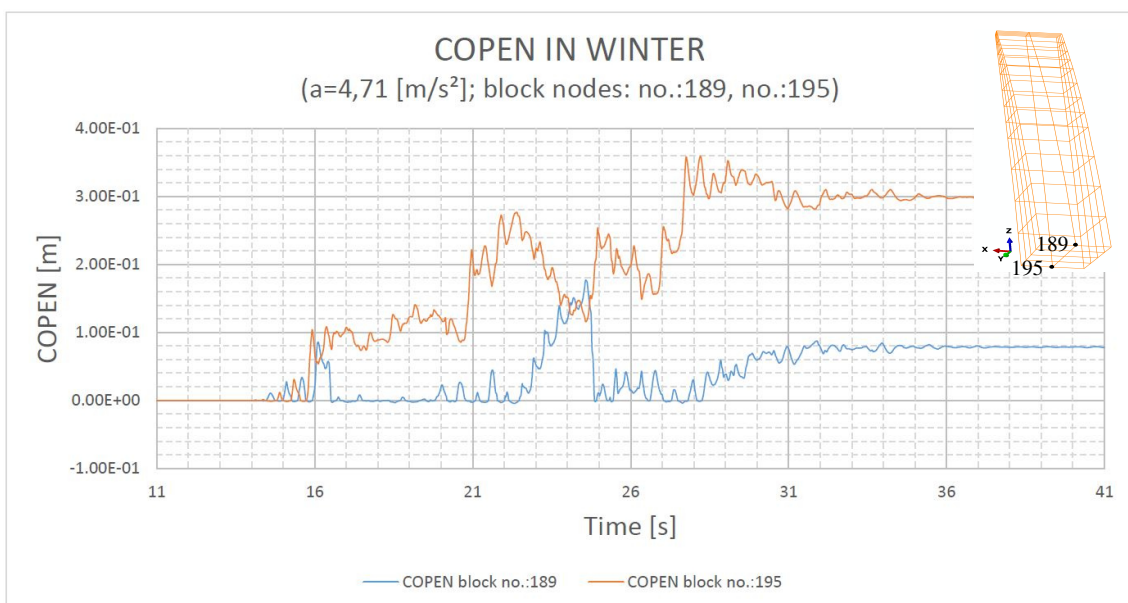
Figure 6-12   Comparison of the joint opening of block nodes 189 and 195 in winter (for example at earthquake acceleration a=4,71 [m/s²])

6.4.5 Comparison of the selected block nodes at the block side face

The following two pictures depict the comparison of the joint opening of the upstream located node number 27 and the downstream located node number 7 (see also Figure 6-9). The blue and red line represent the joint opening (COPEN at the ordinate) at the corresponding time step (abscissa). The underlying earthquake acceleration of the two diagrams is 4,71 [m/s²].

Subsequently you can see that the joint opening respectively the joint closing of both nodes occurs always at the same time step. Considering only those two nodes the modelled block would fall out because of the described opening and closing pattern.

Figure 6-13   Comparison of the joint opening of block nodes 27 and 7 in winter (for example at earthquake acceleration a=4,71 [m/s²])

Figure 6-14 shows a more detailed view (bigger scale) of Figure 6-13 between time step 29 and 34. The diagram shows that the joint moving of both nodes is simultaneously. In conjunction with Figure 6-12 (joint opening at the block foot) the block is supposed to fall out if the joint is open at the same time at all four nodes (195, 189, 11 and 35). Exemplarily this happens at time step 31,30 [s]. At this time step also the joint at node numbers 155 and 150 (Figure 6-15) is open and this situation underlines the assumption that supposes the block to fall out.
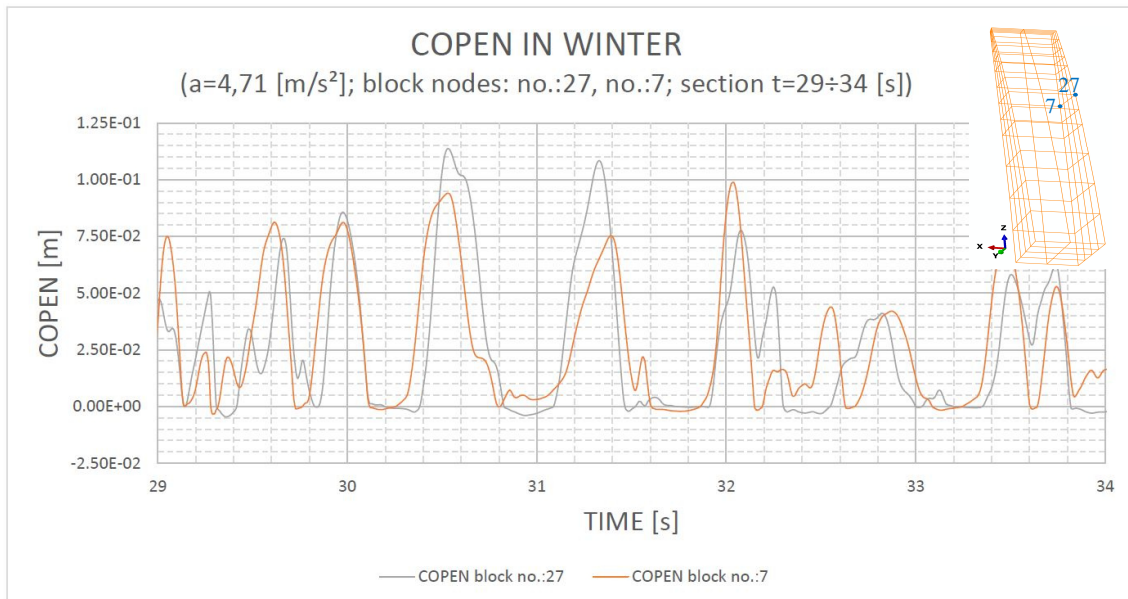
Figure 6-14   More detailed view of Figure 6-13 between time step 29 and 34
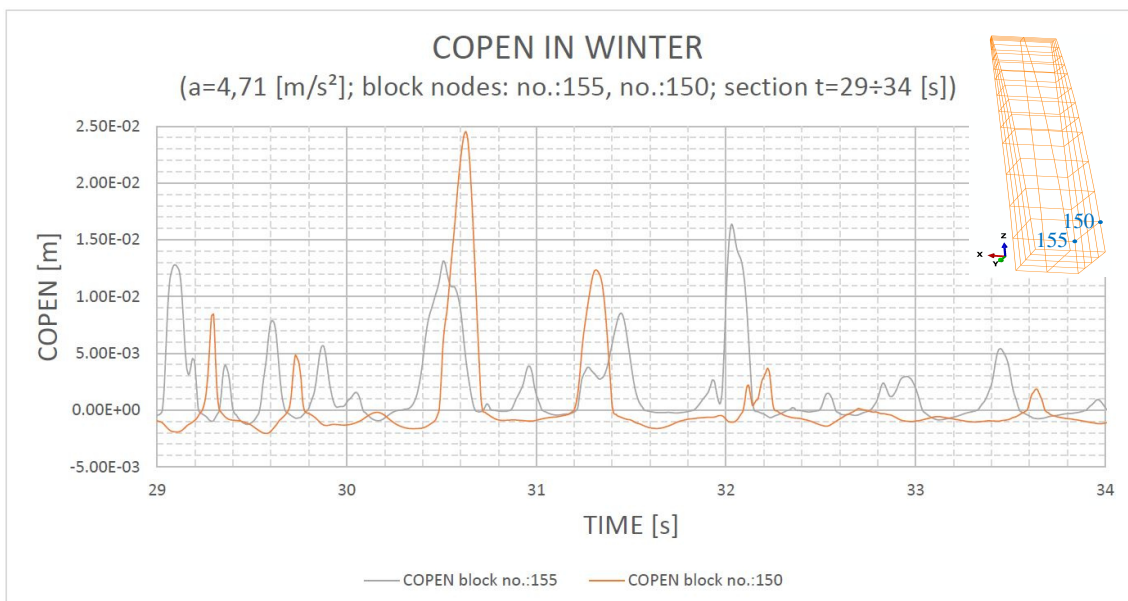
Figure 6-15   Detailed view of the joint opening between time step 29 and 34 of node 155 and 150

The following picture displays why the system isn´t failing. The block stays in the wall at the foot. It shows that during the joint opening of nodes 155 and 150 (Figure 6-15) the nodes 11 and 35 (Figure 6-16) still have contact. Therefor the block can´t fall out.

The above mentioned effect can be observed at every time step during every investigated earthquake acceleration.
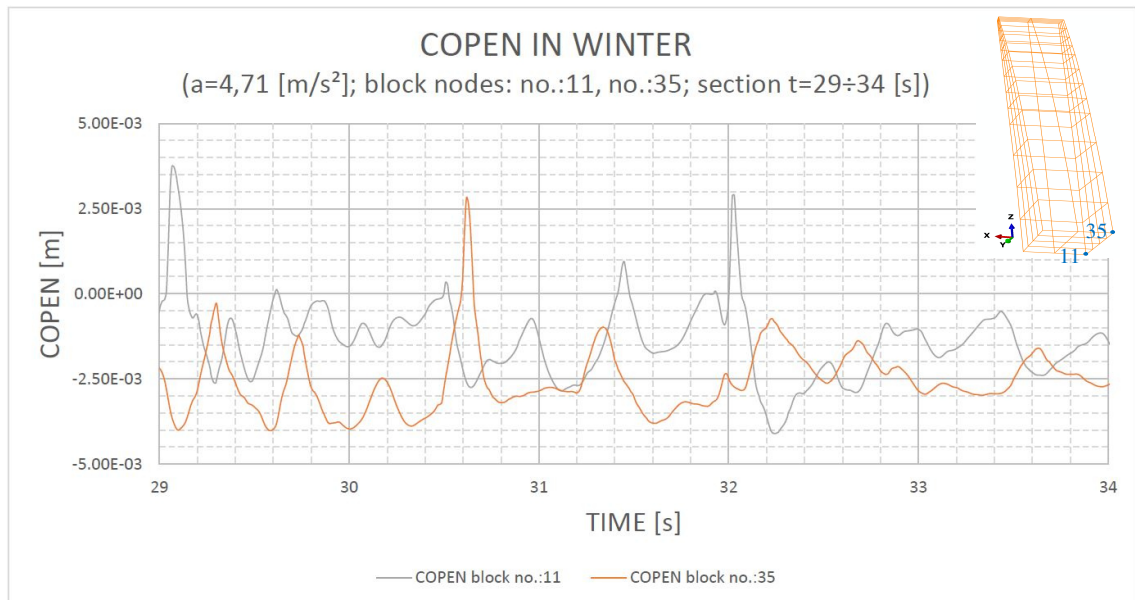
Figure 6-16   Detailed view of the joint opening between time step 29 and 34 of node 11 and 35

6.4.6 Confirmation that the dam-block compound remains

The following diagram shows a comparison between the joint opening (blue line) and the relative tangential motion (displacement - orange line) of the block during the whole earthquake. The maximal displacement is smaller than 0,12 [m] which demonstrates that the construction does not fail. Otherwise the deformation (orange line in Figure 6-17) would increase to infinity.
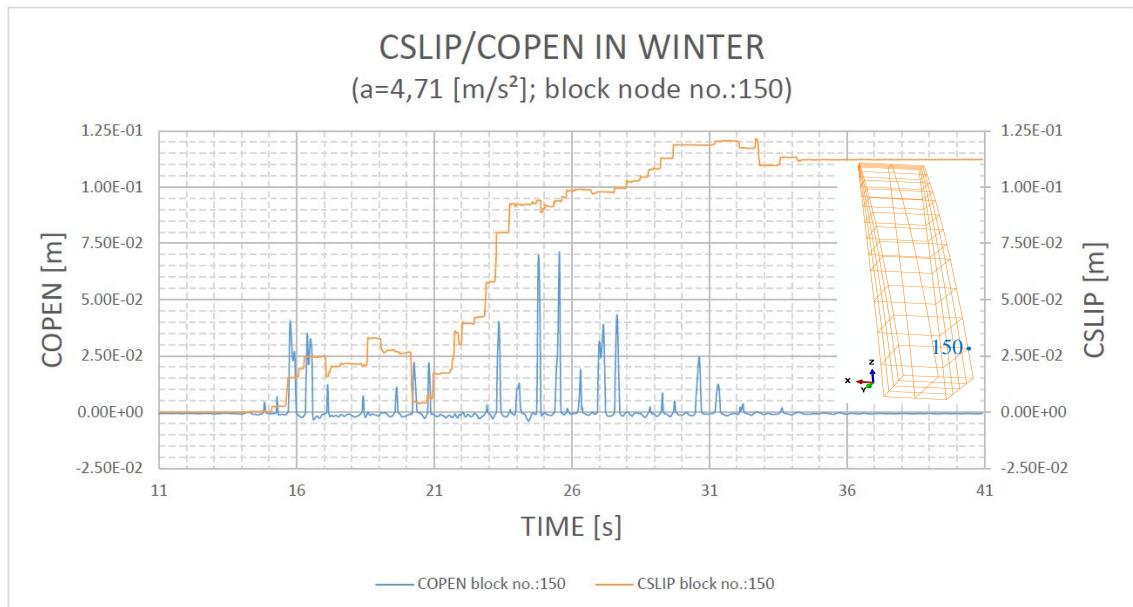
Figure 6-17　　　Confirmation that the construction does not fail (e.g. for node 150 at a= 4,71 [m/s²])

6.4.7 Relative displacement between block and arch dam

Figure 6-18 shows the locations where the relative displacement between block and dam is analysed. Two areas for the evaluation have been chosen. The first area is situated in the block-dam joint at the dam crest and the second in the block-dam joint at the block foot.
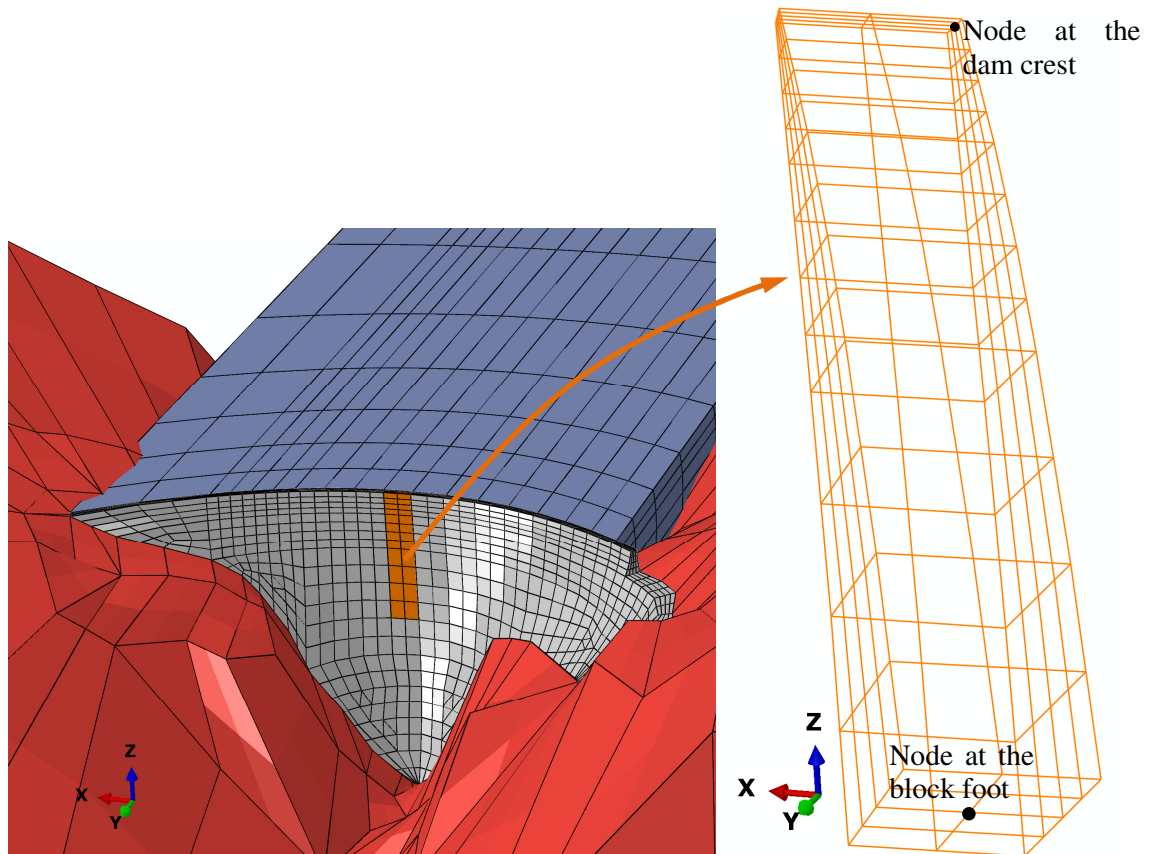
Figure 6-18   Location where the relative displacement is analysed

The following tables (Table 6-7, Table 6-8, Table 6-9 and Table 6-10) depict the relative displacement at the two analysed points in the block-dam joint (Figure 6-18). In all four tables $u_{2,max,ti}$ represents the maximum displacements. Next to the displacement the associated time steps are displayed at which the block respectively the dam moving occurs. The last two columns display the maximum relativ displacement between block and dam at the defined analysing points and their associated time steps.

Table 6-7 and Table 6-8 (one for summer temperature and on for winter temperatur) contain the analyses of the relative displacement at the block foot at the associated time steps. The relativ displacement between the block and the dam is zero or near to zero.

Relative displacement (block foot to arch dam) in summer								
h_{Block} [m]	φ [°]	a [m/s²]	$u_{2,max,ti}$ Block [m]	t_i [s]	$u_{2,max,tk}$ Dam [m]	t_k [s]	Δu_{max} [m]	t_k [s]
100	30	1.57	-0.020	17.51	-0.020	17.51	0.000	15.17
100	30	3.14	0.028	24.18	0.073	28.40	0.001	15.28
100	30	4.71	0.069	24.19	0.132	24.19	0.000	14.84

Table 6-7   Relative displacement between block foot and arch dam in summer

Relative displacement (block foot to arch dam) in winter								
h_{Block} [m]	φ [°]	a [m/s²]	$u_{2,max,ti}$ Block [m]	t_i [s]	$u_{2,max,tk}$ Dam [m]	t_k [s]	Δu_{max} [m]	t_k [s]
100	30	1.57	-0.037	17.51	-0.037	17.51	0.000	15.16
100	30	3.14	0.002	24.18	0.050	28.40	0.000	15.27
100	30	4.71	0.041	24.18	0.110	24.19	0.000	14.83

Table 6-8   Relative displacement between block foot and arch dam in winter

The last two tables (Table 6-9 and Table 6-10) show the values of the relative displacement at the arch dam crest in summer and in winter. Differently to the relative displacement at the block foot (second last column in Table 6-7 and Table 6-8) the relative motion at the arch dam crest shows results between 0 [m] and 1.655 [m] (second last column in Table 6-9 and Table 6-10).

Relative displacement (block to arch dam crest) in summer								
h_{Block} [m]	φ [°]	a [m/s²]	$u_{2,max,ti}$ Block [m]	t_i [s]	$u_{2,max,tk}$ Dam [m]	t_k [s]	Δu_{max} [m]	t_k [s]
100	30	1.57	0.072	25.97	0.092	25.97	0.000	15.49
100	30	3.14	1.086	22.31	1.248	16.42	0.723	25.97
100	30	4.71	2.032	27.76	1.835	16.42	1.655	22.54

Table 6-9   Relative displacement between block and arch dam crest in summer

Relative displacement (block to arch dam crest) in winter								
h_{Block} [m]	φ [°]	a [m/s²]	$u_{2,max,ti}$ Block [m]	t_i [s]	$u_{2,max,tk}$ Dam [m]	t_k [s]	Δu_{max} [m]	t_k [s]
100	30	1.57	0.024	25.97	0.040	25.97	0.001	28.82
100	30	3.14	1.100	22.31	1.192	16.42	0.779	19.87
100	30	4.71	1.941	28.18	1.770	16.43	1.576	27.87

Table 6-10   Relative displacement between block and arch dam crest in winter

6.4.8 Joint opening with earthquake acceleration 1,57 [m/s²] at defined time step in summer

The following figure shows the joint opening between the defined block (orange) and the arch dam. For this analysis the earthquake load is chosen with 1,57 [m/s²] with summer temperature. The opening face which is pictured at the right side of Figure 6-19 (black) is displayed with a camber of 200. This opening face shows that the joint only opens along half of the height of the block. This analysis gives a value of 0,013 [m] respectively 0,003 [m] for the joint opening at the dam crest at an earthquake acceleration of 1,57 [m/s²] .
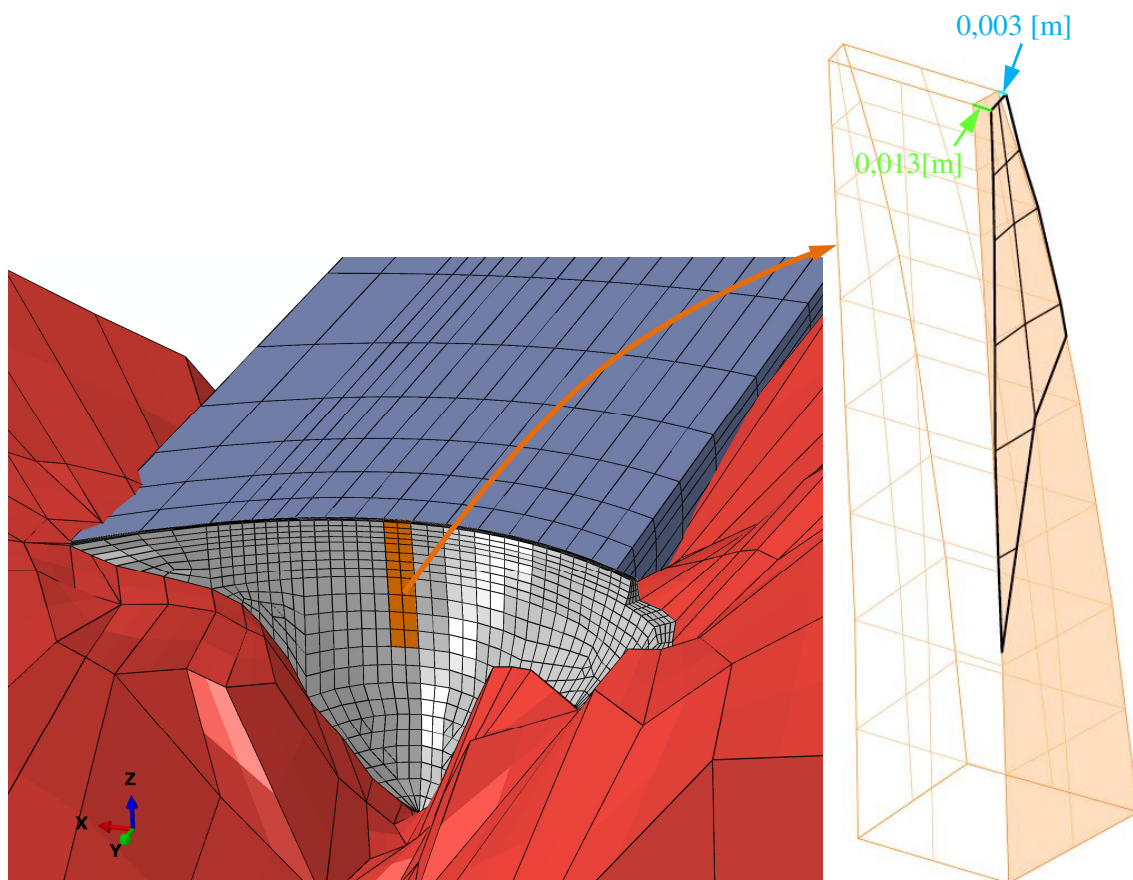
Figure 6-19   Joint opening at earthquake acceleration a=1,57 [m/s²] and time step t=25,38 [s]

6.4.9   Final movement of the block after earthquake loading in summer

Figure 6-20 and Figure 6-21 represent the final movement of the defined block after the earthquake loading in summer. Basis for the final block moving in Figure 6-20 is an earthquake acceleration of a=3,14 [m/s²]. Figure 6-21 underlies an earthquake acceleration of a=4,71 [m/s²].

As mentioned in chapter 5.2.2 the defined boundary conditions which describe the joint behaviour are only the contact behaviour and the friction angle. Due to the earthquake, tensile stresses occur at the block foot face and the block side wall faces.

At both acceleration loads (a=3,14 [m/s²] for Figure 6-20 and a=4,71 [m/s²] for Figure 6-21) the joint at the block foot opens completely and stays open until the end of the earthquake (see also Figure 6-11). If only this behaviour is investigated the system collapses but as mentioned in the previously described chapters the system does not fail because during the earthquake loading the defined block is always in contact with the concrete dam.

In Figure 6-20 (earthquake acceleration of 3,14 [m/s²]) the entire side wall faces are in contact with the adjoining dam. In Figure 6-21 at an acceleration of 4,71 [m/s²] only the lower area of the block stays in contact but this area is big enough to generate sufficient friction.

Both pictures are drawn with a camber of 20.
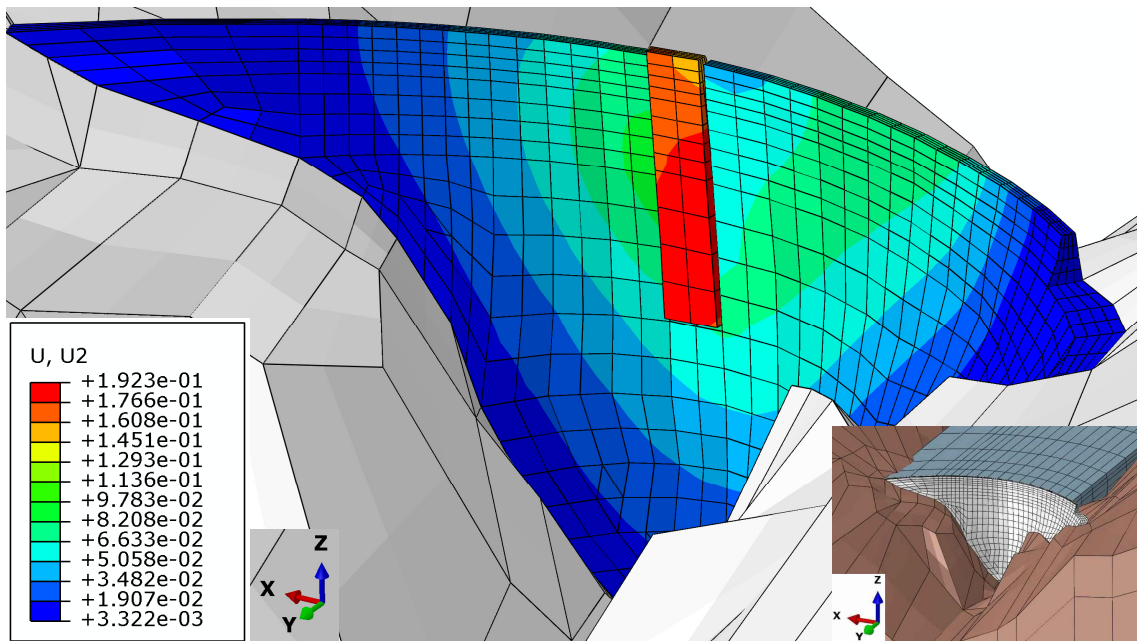
Figure 6-20   Final movement of the block after an earthquake load of a=3,14 [m/s²] in summer
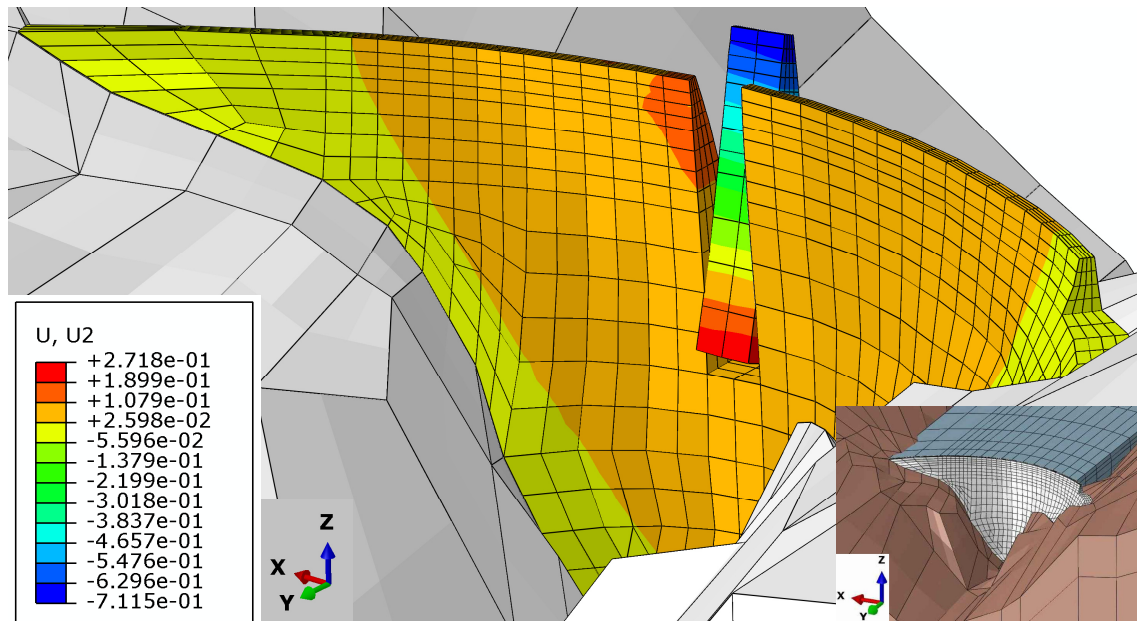
Figure 6-21   Final movement of the block after an earthquake load of a=4,71 [m/s²] in summer

6.5 Acceleration on then dam crest due to different earthquake accelerations

6.5.1 Position where the acceleration verification is done

The subsequent picture shows the point where the accelerations on the top of the dam due to the earthquake load on the dam base is analysed. This evaluation point (green) is situated at the middle cross section of the dam (red) on the crest.
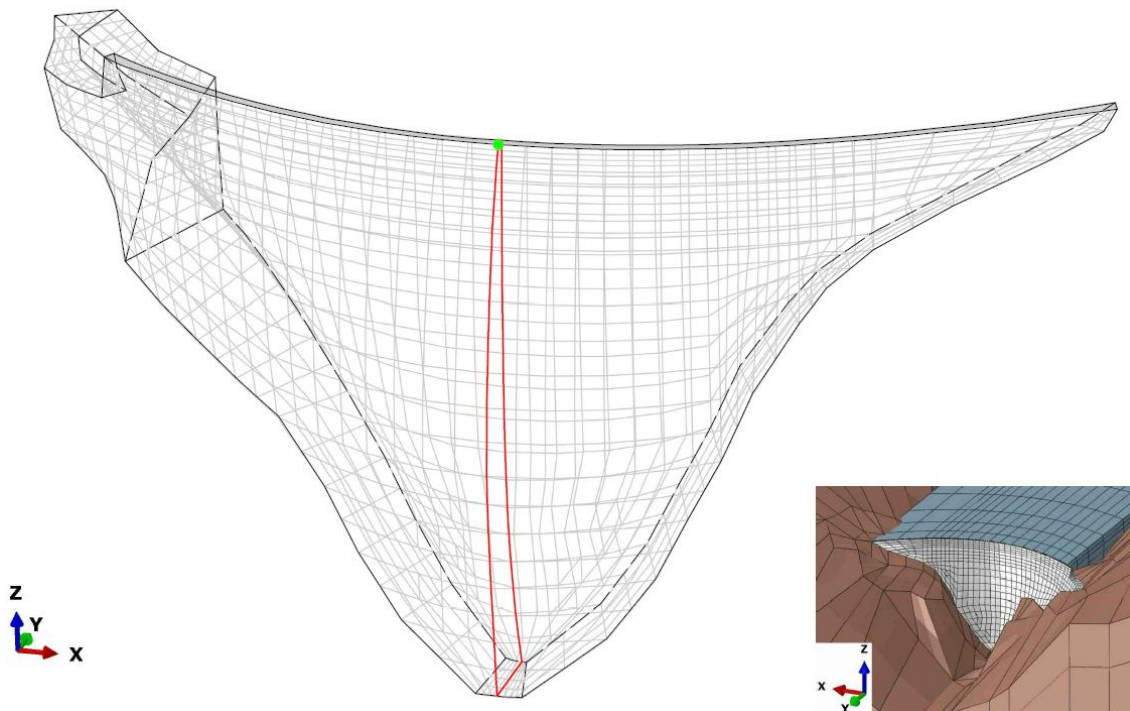
Figure 6-22   Point on arch dam crest where the acceleration is analysed

6.5.2 Relation between the maximum acceleration at the dam crest and the earthquake acceleration at the dam base

A sketch is situated on the right hand side of the following diagram for orientation for which point (green) the corresponding diagram is valid. The evaluation of the acceleration values at the dam crest (green point) happens at 1,57 (dark blue), 3,14 (blue), 4,71 (dark green) and 6,28 (light green) [m/s²] earthquake acceleration. The continuous red line shows the positive accelerations which are in direction of the flow of the water and the red dashed line represents the negative accelerations which are against the direction of the flow. The different evaluation values ($a_{2,i}$) which are the basis for the diagram are written down in Table 6-11.
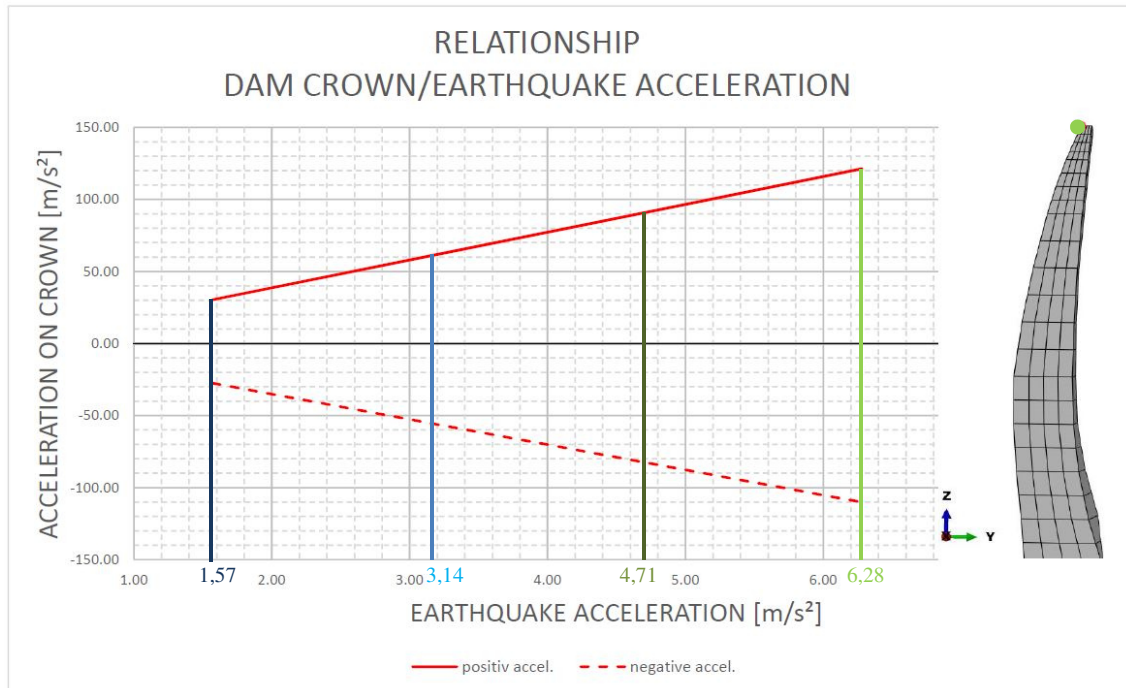
Figure 6-23   Relationship between the acceleration on dam crest and the earthquake acceleration

Finally Table 6-11 displays the base values (a and $a_{2,max}$) of the diagram above. In addition also the amplification values ($A_{2,i}$) are listed. The results for the calculation of the amplifications are nearly identical at each earthquake load. Therefore every earthquake acceleration at the base can be multiplied with this value to get the acceleration at the defined point (Figure 6-22) on top (crest). In conclusion it can be said that the amplification from the foot to the arch dam top (crest) is nearly 18 and has validity for negative and positive acceleration.

ACCELERATION AND AMPLIFICATION				
a [m/s²]	$a_{2,max}$ [m/s²]	$A_{2,max}$ [-]	$a_{2,min}$ [m/s²]	$A_{2,min}$ [-]
1.57	30.31	19.30	-27.55	-17.55
3.14	60.64	19.31	-55.09	-17.54
4.71	90.96	19.31	-82.62	-17.54
6.28	121.29	19.31	-110.16	-17.54

Table 6-11   Acceleration and amplification due to earthquake loading

7 Conclusion

The goal of this master´s thesis is to get an overview of the behaviour of a double curved arch dam which is called the "Luzzone dam" and is situated in the Italian speaking area of Switzerland. The basis for the used numerical model are data of the "13th Benchmark Workshop on the Numerical Analysis of Dams" which are provided from the authors of this workshop. This data consist of the base model, material properties and all needed boundary conditions.

The evaluation of the previously described mentioned concrete dam is done with the finite element software Abaqus. The provided model is generated with the finite element software DIANA and therefore the data have to be converted. Furthermore the mesh size of the used model is refined and much smaller than the provided one. All comparisons are done with evaluations from calculations of a finite element model with bigger mesh size. Additionally this fact gives an overview of the accuracy between the evaluations with the different mesh sizes. The conclusion of this investigation part is, that the comparisons show no relevant deviations.

To get results which allow to assess the real dam behaviour the main influences regarding to the loading are considered. These influences can be static or dynamic. For static loading, next to the self-weight also the hydrostatic pressure and furthermore the silt pressure are considered respectively defined. The summer and winter periods are taken into account with different temperature loadings. For dynamic loading an acceleration time history which describes the earthquake developing is considered. The scaling of this time history is done with different acceleration values (which are proportional) to get a comparison between the consequences at different earthquake excitations. To take the influence of the reservoir during dynamic action into account the water is defined as a volume part with a non-reflecting face on the reservoirs end. The acoustic impedance at the reservoir´s side faces and also on the reservoir´s bottom face are neglected. This fact leads to an underrating of the factors of safety.

All static results are the outcome of a linear calculation method. Regarding the dynamic evaluations all results are calculated in a nonlinear way because of the calculation method with earthquake time histories. As mentioned above these time histories are scaled with different acceleration values and therefore different earthquake strengths are simulated.

Normally the entire concrete dam is constructed with joints and grouted to act as a monolith. In contrast to this in this thesis also the behaviour of a single defined block is investigated. This definition should evaluate the effect of the construction joints which form during the building process because of operational reasons. In the end the evaluations show, that the used numerical model does not fail and the block stays in place. This is because during every defined earthquake loading the block faces have enough contact with the dam and therefore enough resistance against system collapsing as long as there is no failure of concrete in the block itself. Additional to that, in the present case the tensile stresses in the arch dam wall are not high enough for failure of the system.

The last analysing chapter of this thesis is the amplification from the arch dam foot to the top of the dam. In those calculations the acceleration at the concrete dam foot and the acceleration at the dam crest is evaluated. In all verifications the amplification factor is nearly 18.

LIST OF FIGURES

LIST OF TABLES

LIST OF SYMBOLS

m_i	Concentrated mass
$\ddot{u}_i$	Acceleration of the concentrated mass
$\dot{u}_j$	Velocity
u_j	Displacement
c_{ij}	Viscous damping (proportional to velocity)
k_{ij}	Spring rate
$p_i(t)$	Loading
[M]	Mass matrix
[C]	Damping matrix
[K]	Stiffness matrix
$\{\ddot{U}\}, \{\dot{U}\}, \{U\}$	Acceleration, velocity and displacement vector
$\{P(t)\}$	Load vector
α	Mass proportional factor
β	Stiffness proportional factor
ω_i, ω_j	Natural frequency
ξ_i	Modal damping

BIBLIOGRAPHY

[1] R. Flesch und H. Pacht, Baudynamik praxisgerecht, Bd. I Berechnungsgrundlagen, Wiesbaden und Berlin: Bauverlag GmbH, 1993.

[2] M. Goldgruber, "Nonlinear Seismic Modelling of Concrete Dams," Graz University of Technology, Graz, Austria, 2015.

[3] Institut für Wasserbau und Wasserwirtschaft, Konstruktiver Wasserbau Grundlagen, Lernbehelf, Graz, Austria, 2011.

[4] A. D. Tzenkov and R. M. Gunn, *Seismic Safety Evaluation of a Concrete Dam Based on Guidelines,* St-Légier-la-Chiésasz, 2015.

[5] D. SYSTEMS, "Abaqus 6.13 Documentation," DASSAULT SYSTEMS, 2013.

[6] M. Goldgruber, S. Shahriari and G. Zenz, "Seismic Safety Evaluation of a Concrete Dam Based on Guidelines," Graz University of Technology, Graz, Austria, 2015.

[7] A. Michael, "Wikipedia, Die Freie Enyklopädie," 16 August 2011. [Online]. Available: https://commons.wikimedia.org/wiki/File:Luzzone_Lago.jpg#/media/File:Luzzone_ Lago.jpg. [Accessed 09 11 2015].

[8] Tschubby, "Wikipedia, Die freie Enzyklopädie," 01 01 2015. [Online]. Available: https://commons.wikimedia.org/wiki/File:Karte_Lage_Kanton_Tessin_2015.png#/me dia/File:Karte_Lage_Kanton_Tessin_2015.png. [Accessed 09 11 2015].

[9] C. Wiki, "CADFEM Wiki," CADFEM GmbH, [Online]. Available: http://www.cae-wiki.info/wikiplus/index.php/Rayleigh-D%C3%A4mpfung. [Accessed 06 07 2016].

[10] J. Giesecke und E. Mosonyi, Wasserkraftanlagen - Planung, Bau und Betrieb, Springer-Verlag Berlin Heidelberg, 2005.

[11] F. K. Wittel, „Eine kurze Einführung in die Finite Elemente Methode," ETH Zürich, Zürich, Schweiz, 2010.

[12] R. Widmann, Die Talsperren Österreichs, Bd. 33, Graz, Austria: Österreichisches Nationalkomitee für Talsperren, 1999.

[13] S. Adhikari, "Damping Modes for Structural Vibration," University of Camebridge, 2000.

[14] B. Weber, Vorlesung - Tragwerksdynamik, Zürich, Schweiz: ETH Zürich, Abteilung für Bauingenieurwesen - Institut für Baustatik und Konstruktion, 2002.

[15] A. K. Chopra, Dynamics of Structures, Theory and Applications to Earthquake Engineering, New Jersy: Prentice Hall, 2012.

[16] Ö. Staubeckenkommision, Erdbebenberechnung von Talsperren, Grundlagen, vol. 1, 2001.

64